Article

Tumour immune rejection triggered by activation of α2-adrenergic receptors

https://doi.org/10.1038/s41586-023-06110-8

Received: 30 July 2021

Accepted: 20 April 2023

Check for updates

Jingjing Zhu[1,2,3]✉, Stefan Naulaerts[1,2], Loubna Boudhan[1,2,3], Manon Martin[2,4], Laurent Gatto[2,4] & Benoit J. Van den Eynde[1,2,3,5]

Immunotherapy based on immunecheckpoint blockade (ICB) using antibodies induces rejection of tumours and brings clinical benefit in patients with various cancer types[1]. However, tumours often resist immune rejection. Ongoing efforts trying to increase tumour response rates are based on combinations of ICB with compounds that aim to reduce immunosuppression in the tumour microenvironment but usually have little effect when used as monotherapies[2,3]. Here we show that agonists of α2-adrenergic receptors (α2-AR) have very strong anti-tumour activity when used as monotherapies in multiple immunocompetent tumour models, including ICB-resistant models, but not in immunodeficient models. We also observed marked effects in human tumour xenografts implanted in mice reconstituted with human lymphocytes. The anti-tumour effects of α2-AR agonists were reverted by α2-AR antagonists, and were absent in *Adra2a*-knockout (encoding α2a-AR) mice, demonstrating on-target action exerted on host cells, not tumour cells. Tumours from treated mice contained increased infiltrating T lymphocytes and reduced myeloid suppressor cells, which were more apoptotic. Single-cell RNA-sequencing analysis revealed upregulation of innate and adaptive immune response pathways in macrophages and T cells. To exert their anti-tumour effects, α2-AR agonists required $CD4^+$ T lymphocytes, $CD8^+$ T lymphocytes and macrophages. Reconstitution studies in *Adra2a*-knockout mice indicated that the agonists acted directly on macrophages, increasing their ability to stimulate T lymphocytes. Our results indicate that α2-AR agonists, some of which are available clinically, could substantially improve the clinical efficacy of cancer immunotherapy.

ARs are a class of G-protein-coupled rece ptors. They are subdivided into two types (α and β) and several subtypes on the basis of their structure, pharmacology and signalling mechanisms[4]. β-ARs signal through G_s to increase adenylate cyclase activity and cyclic AMP (cAMP) levels, resulting in activation of protein kinase A (PKA) and downstream transcription factors[5,6]. By contrast, α2-ARs signal through G_i to inhibit adenylate cyclase, reducing cAMP levels and PKA activity. Although ARs have a well-described role in the sympathetic nervous system, they are also expressed in other tissues and their function outside the nervous system is not well known, particularly for α2-AR. A number of immunosuppressive mechanisms acting in the tumour microenvironment (TME) to repress anti-tumour immune responses increase cAMP by activating adenylate cyclase. These include β-AR signalling but also adenosine receptor signalling, and prostaglandin signalling through EP2 and EP4 prostanoid receptors[7–9]. Relevant antagonists are being developed for cancer immunotherapy. We reasoned that α2-AR agonists, by inhibiting adenylate cyclase, might be more potent than such antagonists because they could simultaneously block multiple immunosuppressive pathways that increase cAMP.

Tumour growth inhibition by α2-AR agonists

To evaluate the role of α2-AR in cancer progression, we treated mice bearing MC38 colon tumours with different α2-AR agonists and antagonists. We initially tested guanabenz (GBZ) and observed a substantial reduction in tumour growth and an increase in mouse survival (Fig. 1a and Extended Data Fig. 1a). We then observed similar effects with two other a2-AR agonists, clonidine (CLD) and guanfacine (GFC) (Fig. 1a and Extended Data Fig. 1a,b). By contrast, the α2-AR antagonists (yohimbine (YHB) and phentolamine (PHE)) did not affect tumour growth (Fig. 1a). We next tested 11 additional transplanted tumour models: melanomas B16F1 (Fig. 1b) and B16F10 (Extended Data Fig. 1a,c), colorectal carcinoma MC38-OVA, lung carcinoma TC-1, hepatocellular carcinoma Hepa 1-6, T cell lymphoma E.G7-OVA, myeloma J558, mammary carcinoma TS/A, renal carcinoma Renca, fibrosarcoma CMS5a and mammary carcinoma 4T1 (Extended Data Fig. 1c). In all of these models, we observed a similar inhibition of tumour growth after treatment with α2-AR agonists.

Notably, several of the models that responded to α2-AR agonists are well known to be resistant to ICB, such as TC-1 (Extended Data Fig. 1c),

[1]Ludwig Institute for Cancer Research, Brussels, Belgium. [2]de Duve Institute, UCLouvain, Brussels, Belgium. [3]Walloon Excellence in Life Sciences and Biotechnology, Brussels, Belgium. [4]Computational Biology and Bioinformatics, UCLouvain, Brussels, Belgium. [5]Ludwig Institute for Cancer Research, Nuffield Department of Medicine, University of Oxford, Oxford, UK. ✉e-mail: jingjng.zhu@uclouvain.be

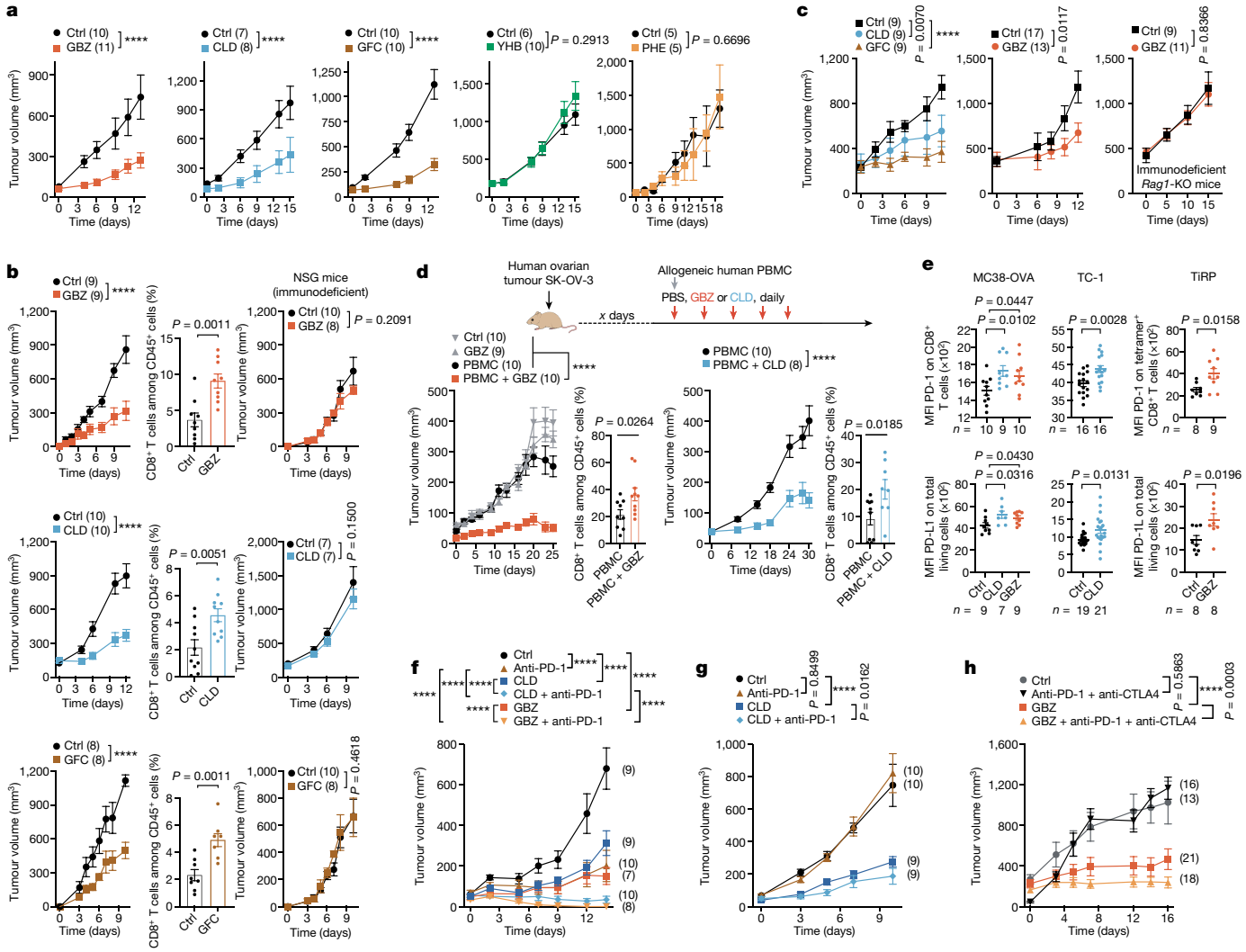

Fig. 1 | α2-AR agonists induce immune-mediated tumour regression in multiple models. a, Progression of MC38 colon carcinomas in mice treated with vehicle (Ctrl), the α2-AR agonists GBZ, CLD or GFC, or the α2-AR antagonists YHB or PHE. **b**, Progression of B16F1 melanomas in immunocompetent (left) or immunodeficient (NSG, right) mice treated with vehicle, GBZ, CLD or GFC. $CD8^+$ T cell infiltration was determined using flow cytometry analysis of tumours at the time of euthanasia (middle). **c**, Progression of induced melanomas in WT or immunodeficient TiRP mice treated with vehicle, GBZ, CLD or GFC. **d**, Progression and $CD8^+$ T cell infiltration of human ovarian cancers SK-OV-3 in NSG mice treated with vehicle, GBZ or CLD after adoptive transfer of allogeneic human PBMCs. **e**, Expression of PD-1 on tumour-infiltrating $CD8^+$ T cells (top) and of PD-L1 on total living cells (bottom) from MC38-OVA, TC-1 and TiRP tumours in mice treated with CLD or GBZ. MFI, median fluorescence intensity. **f**–**h**, Progression of MC38-OVA (**f**), TC-1 (**g**) and induced TiRP tumours (**h**) in mice treated with GBZ, CLD, ICB (anti-PD-1 or anti-PD-1 + anti-CTLA4 antibodies) or combinations. Treatments started on day 0 (7 days after tumour implantation; **a**,**b**,**f** and **g**) or when tumours were established as indicated (**c**,**d** and **h**). Drugs were administered daily by i.p. injection at 5 mg per kg (GBZ, CLD, YHB, PHE) or 2 mg per kg (GFC). Anti-CTLA4 (40 μg) and/or anti-PD-1 (200 μg) antibodies (i.p.) were given 1 day before the first injection of α2-AR agonists, then twice a week. The number of mice is indicated in brackets. Data are mean ± s.e.m. from one representative experiment out of at least two, except for **c**,**f** and **g**, for which all mice are shown, and for **h**, for which data are pooled from two independent experiments. *P* values were calculated using ordinary two-way analysis of variance (ANOVA) (**a**–**d** and **f**–**h**) and unpaired two-tailed *t*-tests (bar graphs in **b**,**d** and **e**); ****$P < 0.0001$.

B16F1 (Fig. 1b), B16F10 (Extended Data Fig. 1a,c) and B16F10-OVA (Extended Data Fig. 1d). We further tested α2-AR agonists in the TiRP model of induced autochthonous melanoma, which was shown to resist all forms of immunotherapies[10,11]. All three α2-AR agonists showed anti-tumour effects in the TiRP model when used as monotherapies (Fig. 1c). Inhibition was even stronger when treatment started with smaller tumours (Extended Data Fig. 1e).

This effect appeared not to result from a direct action of α2-AR on tumour cells, as it was observed equally in tumour models that expressed very different levels of α2-AR (Extended Data Fig. 2a), and no direct growth inhibition was observed when tumour cells were treated with α2-AR agonists in vitro (Extended Data Fig. 2b,c). Instead, tumour growth inhibition was immune mediated, as it was not observed in immunodeficient *NOD/Scid/Il-2rg*$^{-/-}$ (NSG) mice (Fig. 1b). Accordingly, tumours from immunocompetent treated mice contained increased numbers of infiltrating $CD8^+$ T lymphocytes (Fig. 1b and Extended Data Fig. 2d). Similarly, there was no effect of GBZ in TiRP mice in the *Rag1*-knockout immunodeficient background, confirming a lymphocyte-mediated mechanism of action (Fig. 1c).

To investigate the therapeutic effect of α2-AR agonists on human tumours, we tested them in immunodeficient NSG mice bearing human tumours and reconstituted with human allogeneic peripheral blood mononuclear cells (PBMCs). We injected NSG mice with cells from either human ovarian carcinoma SK-OV-3, human colorectal carcinoma

LS411N or human prostate carcinoma PC-3. Once tumour xenografts were established, we injected human PBMCs and monitored tumour growth. In such models, tumour cells activate a response of human lymphocytes towards allogeneic antigens, which by nature are more immunogenic than tumour antigens. Despite this high immunogenicity, the allogeneic response did not inhibit tumour growth, indicating the presence of immunosuppressive mechanisms in these tumours (Fig. 1d and Extended Data Fig. 3a). Thus, this model is convenient to evaluate therapeutic approaches aimed at modulating immunosuppression in the setting of human lymphocytes confronted to human tumours, without the hurdle of the poor immunogenicity of human tumours in the autologous setting[12]. We next repeated the experiment and started treating mice with GBZ or CLD at the time at which they received human PBMCs. We observed strong anti-tumour effects in all three models, indicating that α2-AR agonists can boost the rejection of human tumours by human lymphocytes (Fig. 1d and Extended Data Fig. 3a,b). Importantly, despite expression of α2-AR by these tumours (Extended Data Fig. 3c), there was no effect in the absence of human PBMCs, confirming that the anti-tumour activity of α2-AR agonists was immune mediated, and indicating that it was effective also on human lymphocytes. Indeed, xenografts from treated mice contained increased amounts of human tumour-infiltrating $CD8^+$ lymphocytes (Fig. 1d). Even though the anti-tumour immune responses of patients with cancer are weaker than the allogeneic responses tested here, these results suggest that the immune-mediated anti-tumour effects of α2-AR agonists could be translated to patients with cancer.

Combination with checkpoint inhibitors

Mice treated with α2-AR agonists showed an increased expression of PD-1 in tumour-infiltrating lymphocytes (TILs) and of PD-L1 on TME cells, in MC38-OVA, TC-1 and TiRP tumours (Fig. 1e). This prompted us to test combinations of α2-AR agonists with ICB. In the MC38-OVA model, which does respond to anti-PD-1, combination of anti-PD-1 with α2-AR agonists showed a strong synergistic anti-tumour effect, leading to complete tumour rejection in most mice (Fig. 1f and Extended Data Fig. 3d,e). In the TC-1 model, which does not respond to anti-PD-1 therapy, the addition of anti-PD-1 to α2-AR agonists slightly improved their anti-tumour effect (Fig. 1g and Extended Data Fig. 3f). Similarly, TiRP melanomas did not respond to combined ICB therapy (anti-CTLA4 + anti-PD-1)[11], but the addition of combined ICB therapy improved the anti-tumour effect of GBZ (Fig. 1h). Similar results were obtained in the CT26 and B16F1 models (Extended Data Fig. 3g,h). Notably, in most of the ICB-resistant models tested, α2-AR agonists alone were already more efficient than ICB therapy.

Target validation of α2-AR

To confirm the on-target effect of α2-AR agonists, we first used the α2-AR antagonist YHB, and found that coinjection of YHB with CLD or GBZ reverted almost completely the immune-mediated anti-tumour effect of these agonists on human tumour xenografts[13] (Fig. 2a). As α2a-AR was the most highly expressed α2-AR subtype in mouse tumours (Extended Data Fig. 3i), we next used *Adra2a*-KO mice[14], which are genetically deficient in α2a-AR (Extended Data Fig. 3j). The anti-tumour effect of CLD and GBZ on MC38 tumours was abolished in *Adra2a*-KO mice, and so was the increased infiltration of $CD8^+$ T cells (Fig. 2b). The anti-tumour effect of α2-AR agonists was also abolished in *Adra2a*-KO mice for three other models tested (MC38-OVA, TC-1 and B16F10-OVA) (Fig. 2c–e). Similarly, no synergistic effect was found for CLD and GBZ when combined with anti-PD-1 treatment in *Adra2a*-KO mice bearing MC38-OVA tumours (Fig. 2f). These results confirmed α2a-AR as the actual target of the agonists in mediating their anti-tumour effects. Notably, the tumours implanted into *Adra2a*-KO mice were wild-type (WT) for *Adra2a*. The fact that CLD and GBZ did not inhibit tumour growth in *Adra2a*-KO mice therefore provided additional evidence that their anti-tumour effect was not linked to a direct action on tumour cells but relied on the host immune system. We further confirmed this notion by observing that the anti-tumour effect of CLD was fully maintained in WT mice bearing *Adra2a*-KO tumour cells (Fig. 2g).

α2-ARs present in the brainstem exert negative feedback on preganglionic neurons of sympathetic nerves, resulting in reduced release of noradrenaline by sympathetic nerves and of adrenaline by adrenal glands[15,16]. This reduced sympathetic tone explains the clinically effective antihypertensive effect of α2-AR agonists such as CLD and GBZ[17]. Several studies have described the immunosuppressive effect of signalling through β2-AR acting on different cells of the TME[18–23]. It was therefore possible that the immune-potentiating effect of α2-AR agonists was indirect, through reduced β2-AR signalling resulting from the reduced sympathetic tone. However, this was excluded by the observation that the anti-tumour effect of GBZ was maintained in mice that were deficient for both the β1- and the β2-ARs[24] (Fig. 2h). We concluded that α2-AR agonists do not act through reduced β2-AR signalling.

We next compared the anti-tumour efficacy of CLD with that of propranolol (PRP)—a β2-AR antagonist. We observed that CLD was more potent than PRP in the CT26 cancer model (Fig. 2i). PRP was previously reported to increase the therapeutic efficacy of ICB in the 4T1 and the B16F10 models, but showed little therapeutic anti-tumour activity as a monotherapy[22,25]. This contrasts with the potent therapeutic effect of α2-AR agonists as a single agent in multiple models, including 4T1 and B16F10 (Extended Data Fig. 1a,c). Like adenosine receptors and several prostaglandin receptors, β2-ARs associate with G_s and increase cAMP production by adenylate cyclase. The increased anti-tumour potency of α2-AR agonists as compared to PRP is therefore consistent with our hypothesis that α2-AR agonists, by inhibiting cAMP production by adenylate cyclase, can block multiple pathways leading to cAMP-mediated immunosuppression.

Role of CD4 and CD8 T cells

We further analysed which immune cells drive the observed anti-tumour immune response, focusing on the MC38-OVA model, partially responsive to anti-PD-1 therapy, and the TC-1 model, an ICB-resistant model, both of which can grow in the C57BL/6J background of the *Adra2a*-KO mice. Given the increased $CD8^+$ TIL infiltration that we observed in tumour models, we first examined whether the α2-AR agonists acted directly on $CD8^+$ T lymphocytes. Treating $CD8^+$ T cells in vitro with α2-AR agonists did not increase T cell proliferation or activation (Extended Data Fig. 4a). In vivo, the anti-tumour effect of CLD required the presence of $CD8^+$ T cells, as it was partly reduced after $CD8^+$ T cell depletion in both models (Fig. 3a). However, $CD8^+$ T lymphocytes were not the primary targets of CLD, because when we adoptively transferred WT OVA-specific OT-I $CD8^+$ T lymphocytes into *Adra2a*-KO mice bearing MC38-OVA tumours, we observed no increase in tumour growth inhibition after treatment with CLD, despite the abundant presence of anti-tumour $CD8^+$ T cells expressing α2a-AR (Fig. 3b). As a control, CLD increased MC38-OVA tumour growth inhibition in WT mice after adoptive transfer of OT-I $CD8^+$ T cells (Fig. 3c).

Besides increased $CD8^+$ T cell infiltration, we also observed an increase in $CD8^+$ T cell activity among TILs (Fig. 3d, Extended Data Fig. 2g). In addition, we observed increased $CD4^+$ T cell infiltration in the tumour, lymph nodes and spleen of CLD-treated mice bearing TC-1 tumours (Fig. 3e). $CD4^+$ T cells were also increased in MC38-OVA tumours after CLD treatment (Extended Data Fig. 4b). Furthermore, blocking lymphocyte trafficking from secondary lymphoid organs to the tumour with FTY720 prevented the anti-tumour effect of CLD (Fig. 3f), while the increased T cell infiltration was reduced in the tumour and maintained in secondary lymphoid organs (Fig. 3e). As $CD8^+$ T cells are required to mediate the anti-tumour effect of α2-AR agonists, this result was not unexpected. However, the increase in

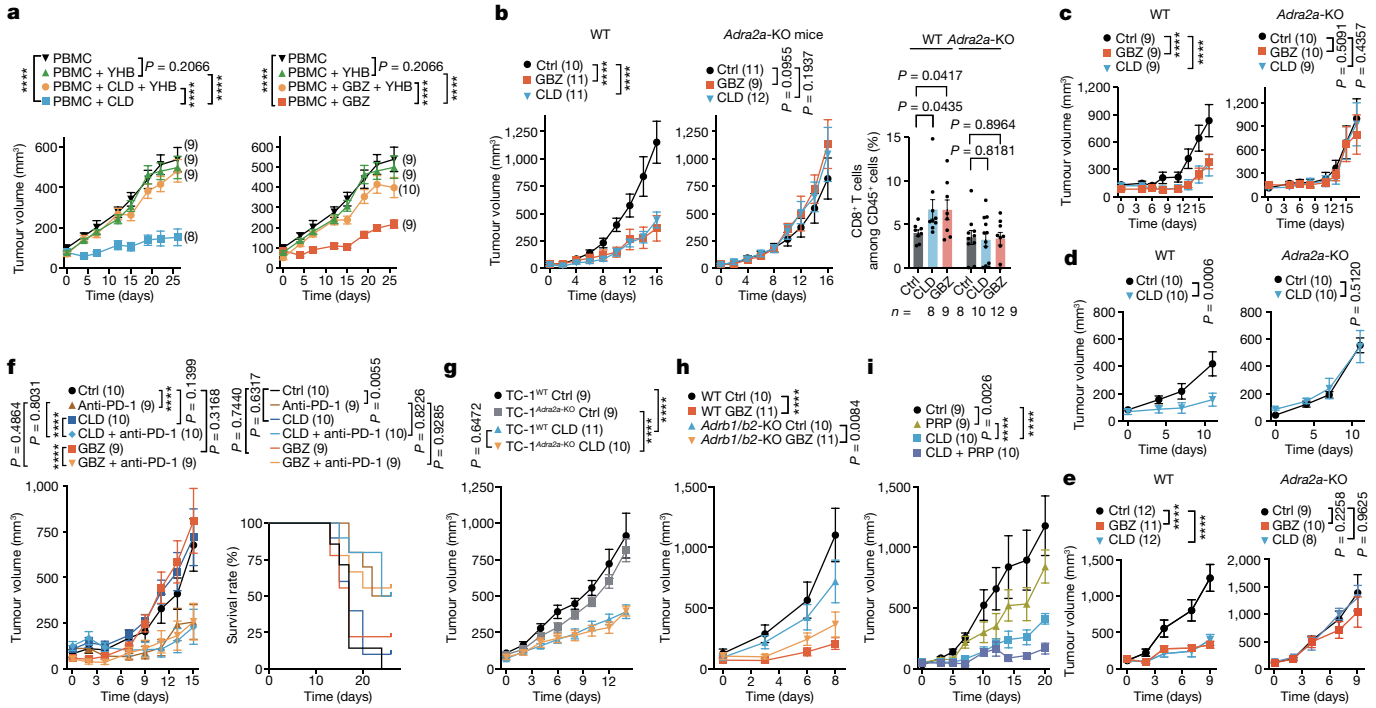

Fig. 2 | Validation of α2-AR as the target mediating the anti-tumour effects of agonists. a, Human LS411N colorectal cancer xenografts in NSG mice reconstituted with human PBMCs and treated with CLD or GBZ, and/or YHB. **b**, MC38 colon carcinomas in WT or *Adra2a*-KO mice treated with vehicle, CLD or GBZ. $CD8^+$ T cell infiltration was analysed as described above. **c**–**e**, MC38-OVA colon carcinomas (**c**), TC-1 lung carcinomas (**d**) and B16F10-OVA melanomas (**e**) in WT or *Adra2a*-KO mice treated with vehicle, GBZ or CLD. **f**, Tumour growth (left) and mouse survival (right) of colon carcinomas MC38-OVA in *Adra2a*-KO mice treated with CLD, GBZ and/or anti-PD-1 as indicated. **g**, Control or *Adra2a*-KO TC-1 lung carcinoma progression in WT mice treated with vehicle or CLD. **h**, MC38 colon carcinomas in WT or *Adrb1/Adrb2*-KO mice treated with vehicle or GBZ. **i**, CT26 colon carcinomas in mice treated with vehicle, PRP, CLD or both. Drugs were administered daily by i.p. injection at 5 mg per kg (GBZ, CLD, PRP) or 10 mg per kg (YHB). Treatments started on day 0, when tumours were well established as indicated on the graphs (**a** and **c**–**h**) or 7 days after tumour implantation (**b** and **i**). Anti-PD-1 (200 μg) antibodies (i.p.) were given 1 day before the first injection of α2-AR agonists, and then twice a week. Data are mean ± s.e.m. from one representative experiment out of at least two performed, except for **e**–**g**, for which all mice are shown. The number of mice per group is indicated in brackets. *P* values were determined using ordinary two-way ANOVA (**a**–**i**) and unpaired two-tailed *t*-tests (bar graphs in **b**) and log-rank (Mantel–Cox) tests were used for the statistical evaluation of mouse survival (**f**, right).

T cell infiltration induced by CLD in secondary lymphoid organs of FTY720-treated mice indicates that α2-AR agonists act not only in the tumour but also in the secondary lymphoid organs. The relative role of each compartment remains to be determined.

Role of MDSCs

We previously observed in the TiRP melanoma model that $CD8^+$ TILs do not survive in the TME owing to apoptosis triggered by Fas ligand (FasL)-expressing polymorphonuclear myeloid-derived suppressor cells (PMN-MDSCs), now also termed pathologically activated neutrophils[26], which were enriched in these tumours[11]. We therefore examined whether α2-AR agonists could prevent TIL apoptosis and favour TIL persistence in this model. We adoptively transferred TCRP1A $CD8^+$ T lymphocytes into TiRP mice bearing induced melanomas, which express the P1A tumour antigen. Agonists of α2-AR favoured the persistence of TCRP1A $CD8^+$ T lymphocytes in the tumours, reduced their apoptosis and increased their activity (Fig. 3g and Extended Data Figs. 2d,f and 4c). Furthermore, α2-AR agonists reduced the number of PMN-MDSCs in the TME of TiRP tumours and increased their apoptosis (Fig. 3g and Extended Data Figs. 2d and 4c,d,e). This resulted in a synergistic therapeutic effect of the combination of α2-AR agonists with adoptive transfer of anti-tumour $CD8^+$ T cells, which was totally ineffective when administered alone in this model (Fig. 3h and Extended Data Fig. 4c). We confirmed that α2-AR agonists also reduced TIL apoptosis and tended to reduce PMN-MDSC numbers in the MC38 tumours, and observed that these effects were absent in *Adra2a*-KO mice (Extended Data Fig. 4f).

To investigate the mechanism of action of α2-AR agonists, we first performed a transcriptomic analysis of bulk RNA from CLD-treated and untreated MC38-OVA tumours from WT and *Adra2a*-KO mice. Gene set enrichment analysis (GSEA) identified an enrichment of genes associated with the innate immune response, cell communication and cytokine response in treated tumours from WT mice (Fig. 3i). Specifically, treated tumours showed signs of immune stimulation, with a high expression of genes relevant for both the innate (such as genes encoding TLR4[27], TLR8, TLR[28] or CD36[29]) and adaptive immune response (encoding CD48[30], ITK[31], CCL22[32], NFATC1 or NFATC2[33]) (Fig. 3j). These signs were absent in CLD-treated tumours from *Adra2a*-KO mice (Fig. 3j). We confirmed using quantitative PCR with reverse transcription (RT–qPCR) the increased expression of *Tlr1*, *Tlr7*, *Tlr8*, *Ifnb1* and *Cxcl13* in tumours treated with CLD and GBZ in WT mice, but not in *Adra2a*-KO mice (Extended Data Fig. 4g).

Further UMAP analysis indicated transcriptomic changes in tumours from CLD-treated mice that were similar to those of GBZ-treated mice, and were absent in tumours from CLD-treated *Adra2a*-KO mice (Extended Data Fig. 4h). Notably, tumours from GBZ-treated *Adra2a*-KO mice showed a distinct transcriptomic profile, consistent with the known effects of GBZ on other pathways such as GADD34[34]. By contrast, the absence of transcriptomic changes induced by CLD in *Adra2a*-KO mice indicated a higher specificity of CLD for α2a-AR in this context. We therefore focused on CLD for the subsequent experiments.

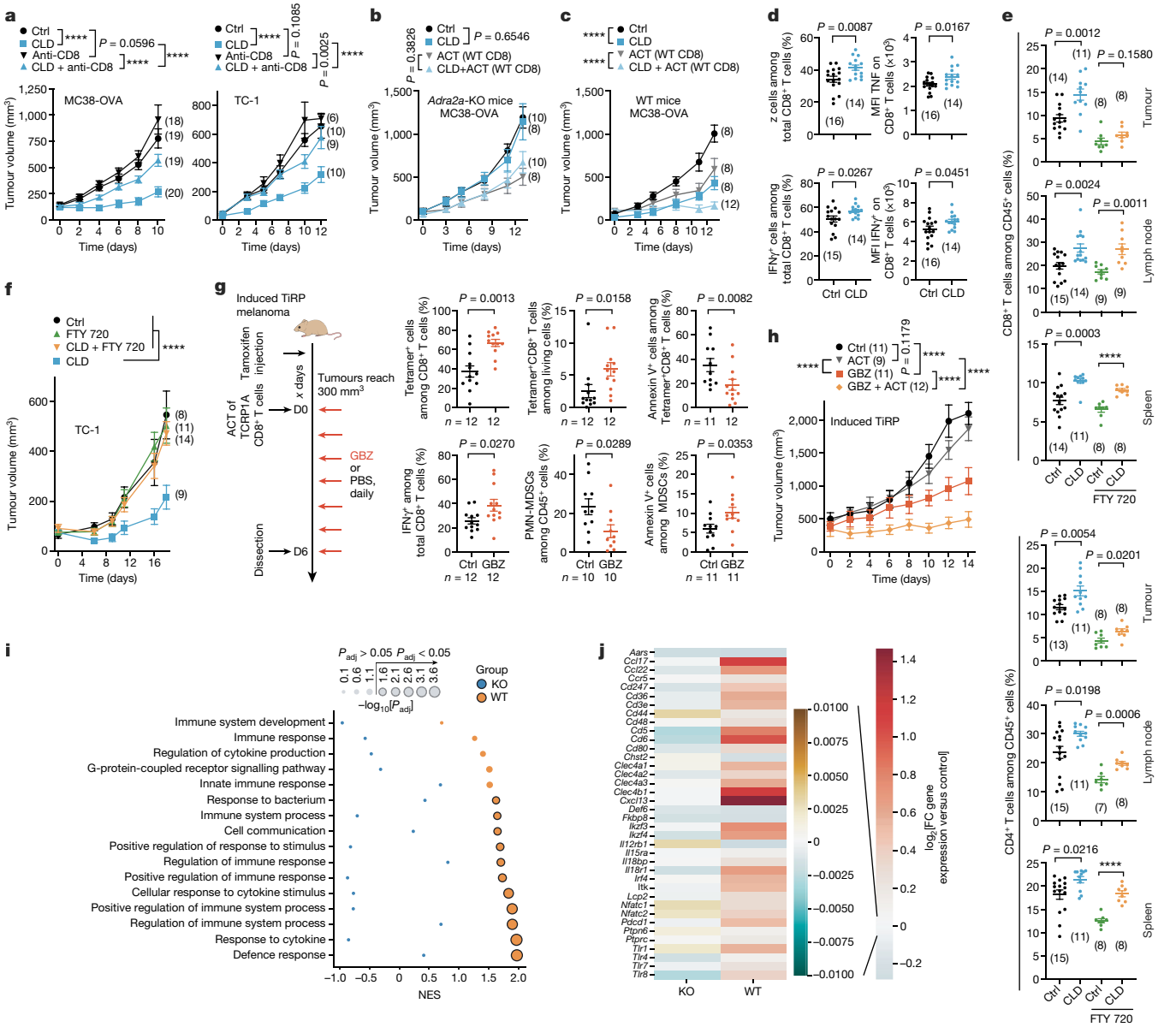

Fig. 3 | Modulation of CD8⁺ T cells and MDSCs by α2-AR agonists. **a**, Tumour progression in mice depleted of CD8⁺ T cells and treated with CLD. **b**, MC38-OVA tumours in *Adra2a*-KO mice receiving adoptive cell transfer (ACT) of 10^7 in vitro activated OVA-specific TCR-OT1 CD8⁺ T cells, and treated with CLD. **c**, The same as in **b** but in WT mice. **d**, Intracellular TNF (top) and IFN (bottom) in CD8⁺ T cells infiltrating TC-1 tumours. **e**, CD4⁺ and CD8⁺ T cell infiltration in TC-1 tumours, lymph nodes and spleens analysed by flow cytometry after 7 days of treatment with CLD and/or FTY720. **f**, Progression of TC-1 tumours in mice treated with CLD, FTY720 or both. **g**, Infiltration, activation and apoptosis of P1A-specific CD8⁺ T cells and PMN-MDSCs in P1A-expressing TiRP melanomas in mice treated with GBZ for 7 days after ACT of 10^7 activated TCRP1A CD8⁺ T cells. **h**, Progression of induced TiRP melanomas after GBZ treatment after ACT as in **g**. **i**, Bulk RNA-sequencing (RNA-seq) GSEA plot for CLD-treated versus untreated MC38-OVA tumours from WT or *Adra2a*-KO mice. Four groups, $n = 3$ per group. Higher normalized enriched scores (NES) indicate upregulation in treated mice. *P* values and the false-discovery rate (FDR) were calculated using a standard GSEA permutation-based approach with 1,000 iterations. Significant enrichments are indicated by a black circle (FDR < 0.05). **j**, Bulk RNA-seq analysis of gene expression in treated tumours versus control after DESeq2 analysis. A magnified colour scale is shown for the KO group. GBZ and CLD were administered at 5 mg per kg i.p. daily. FTY720 was administered at 10 μg per mouse, i.p. daily, starting 1 day before agonist treatment. CD8-depleting antibodies were administered at 500 μg on day −1, then 150 μg weekly. Treatments started on day 0, when tumours were established as indicated. Data are mean ± s.e.m. from one representative experiment out of at least two (**a** (right), **b**,**c**,**f** and **h**), except for **a** (left), **d**,**e** and **g**, for which all mice are shown. *P* values were determined using ordinary two-way ANOVA (**a**–**c**,**f** and **h**) and unpaired two-tailed *t*-tests (**d**,**e** and **g**).

Single-cell transcriptomic analysis

We next performed single-cell transcriptome analysis of the TME of MC38-OVA tumours (Extended Data Fig. 5a and Supplementary Table 1). We confirmed an increased infiltration of CD8⁺ T lymphocytes after CLD treatment (Fig. 4a,b). We also observed a decrease in the cell population expressing neutrophil markers, which might correspond to the PMN-MDSCs that we identified using flow cytometry. The most abundant population in the TME of these tumours was macrophages, which represented more than 87% of CD45⁺ cells (Fig. 4a,b). These macrophages clustered into five different subsets (Fig. 4a and Extended Data Fig. 5b,c). After CLD treatment, the dominant cluster macrophage-3 was almost entirely replaced by cluster macrophage-1, whereas the other clusters were moderately altered

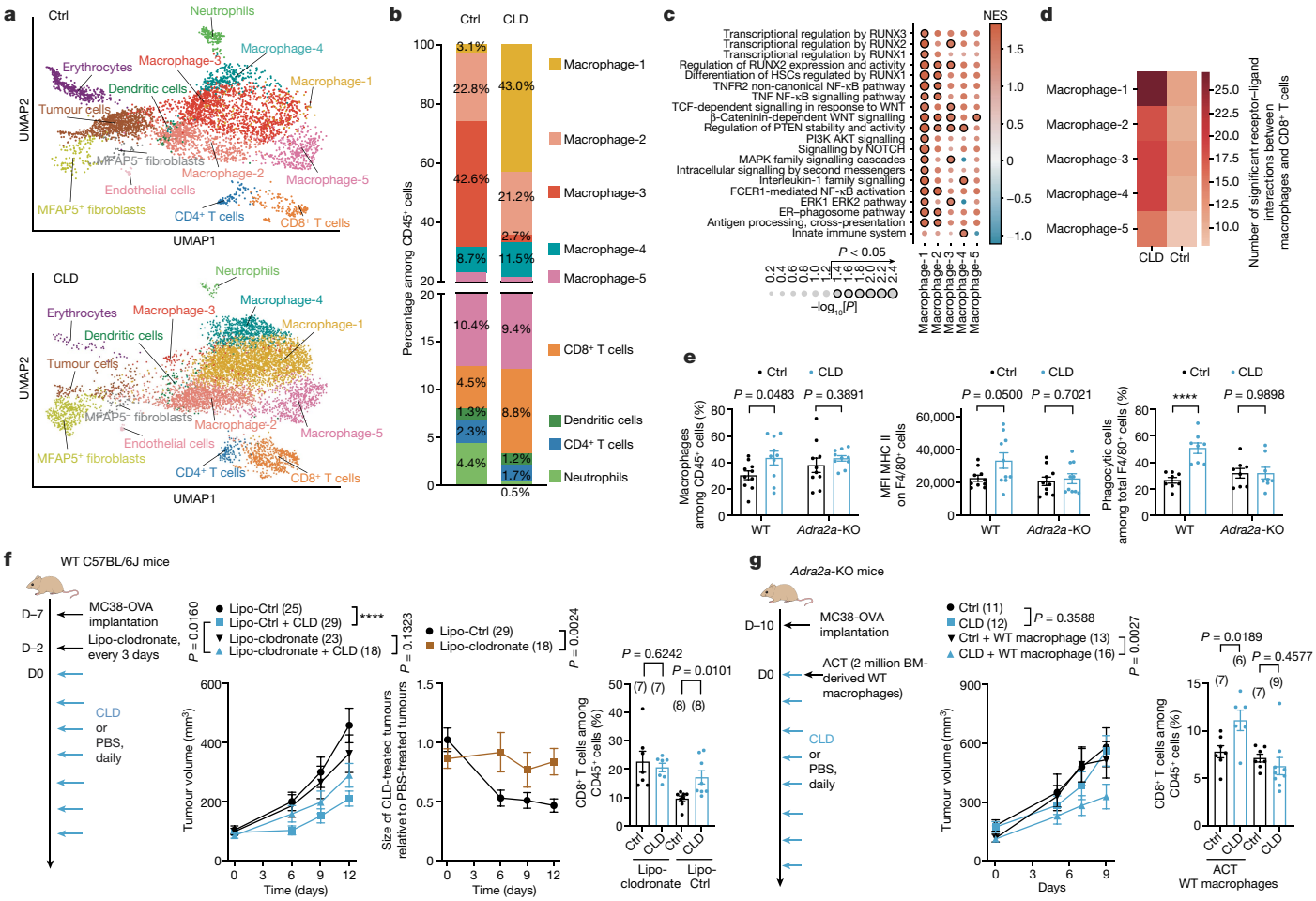

Fig. 4 | Role of macrophages in the anti-tumour effect of α2-AR agonists. **a**, Uniform manifold approximation and projection representation of single cell RNA-seq (scRNA-seq) analysis of untreated (left) and CLD-treated MC38-OVA tumours (right); pools of 10 mice per group. Leiden clusters were identified using PhenoGraph (number of neighbours = 25, number of principal components = 26). **b**, The relative abundances of immune cells per cluster. Cell identities were assigned on the basis of published lists of markers (Supplementary Table 1). **c**, Set enrichment per population for relevant pathways. Significant terms are indicated by a black circle. The marker size represents the *P* value and the colour intensity indicates the normalized enrichment score. *P* and FDR values were obtained by randomly permutating gene ranks 1,000 times and testing using the GSEA approach. ER, endoplasmic reticulum; HSCs, haematopoietic stem cells. **d**, Receptor–ligand interactions between macrophages (donor) and CD8$^+$ T cells (receptor) identified by CellPhoneDB. **e**, Infiltration ($n = 10$), surface MHC II expression ($n = 10$) and phagocytic activity ($n = 8$) of TME macrophages from WT or *Adra2a*-KO mice treated with CLD. **f**, Progression of MC38-OVA tumours in macrophage-depleted mice treated with CLD (left). Middle, the relative size of CLD-treated tumours compared with PBS-treated tumours (individual tumour volume (CLD group)/mean tumour volume (Ctrl group)). Right, T cell infiltration of MC38-OVA tumours in macrophage-depleted mice treated with CLD. Notably, the apparent increase in CD8$^+$ T cells in clodronate-treated mice is only relative and results from macrophage depletion. Clodronate liposomes (lipo) were administered as 150 µl (7 mg ml^{-1}) every 3 days starting 2 days before CLD. **g**, Progression of MC38-OVA tumours in *Adra2a*-KO mice treated with CLD after adoptive transfer (ACT) of WT bone marrow (BM)-derived macrophages (left). Right, CD8$^+$ T cell infiltration of MC38-OVA tumours in *Adra2a*-KO mice treated with CLD after ACT of WT bone-marrow-derived macrophages. CLD was administered i.p. at 5 mg per kg daily. Clodronate liposomes were administered as 150 µl every 3 days starting 2 days before CLD treatment. Data are mean ± s.e.m., pooled from at least two independent experiments, with $n > 5$ per group. *P* values were determined using ordinary two-way ANOVA (**f**,**g**) and unpaired two-tailed *t*-tests (bar graphs in **e**–**g**).

(Fig. 4b). The clusters macrophage-1 and -3 expressed a similar pattern of genes, but with differences in expression levels (Extended Data Fig. 5c). Macrophage-1 showed an M1-macrophage-like transcriptional profile with high expression of MHC-class-II-related genes (*H2-eb1* and *H2-ab1*) and proinflammatory genes (*Ccl2*, *Ccl3*, *Cxcl2* and *Ccl4*), and was similar to the described *C1QC*$^+$ population of tumour-associated macrophages, which were involved in phagocytosis and antigen presentation[35]. The macrophage-3 cluster shows high expression of *Ccrl2* and *Cd83*, and expresses several proinflammatory genes (*Ccl2*, *Ccl3*, *Cxcl2* and *Ccl4*) similarly to macrophage-1. However, as compared to macrophage-1, macrophage-3 expresses lower levels of MHC-class-II-related genes (*H2-eb1* and *H2-ab1*), as well as *Adgre1* (encoding F4/80) and *Itgam* (encoding CD11b). The major shift from macrophage-3 to macrophage-1 that was induced by CLD treatment might reflect an increased proportion of activated macrophages able to phagocytose and present antigens. Consistent with this hypothesis, a GSEA pathway analysis suggested that CLD treatment increased overall macrophage function, with enhanced antigen processing/cross-presentation and endoplasmic reticulum–phagosome pathways, particularly in the macrophage-1 cluster (Fig. 4c). RUNX-family signalling was also increased with CLD, indicating a regulation of myeloid lineage differentiation[36]. The CLD-induced increased expression of several MHC-class-II-related genes, including *Cd74*, *H2-eb1* and *H2-aa*, was confirmed mostly in the macrophage-1 cluster (Extended Data Fig. 5d). These results suggested that CLD not only increased the number of cells in the macrophage-1 cluster, but also improved their ability to

present antigens and interact with T cells. Consistent with this, using the CellPhoneDB receptor–ligand database, we observed a large increase in the number of significant interactions between macrophages and $CD8^+$ T cells after CLD treatment (Fig. 4d). This increase coincided with a significant enrichment in the expression of pathways linked to $CD8^+$ T cell activation (Extended Data Fig. 5e). We found similar transcriptomic changes in macrophages infiltrating TC-1 lung tumours in mice treated with CLD (Extended Data Fig. 5f). Together, these results suggested a key role of macrophages in mediating the effects of CLD.

Involvement of macrophages

We next confirmed expression of α2a-AR by macrophages, MDSCs and $CD8^+$ T cells from the TME of MC38-OVA tumours (Extended Data Fig. 6a). After CLD treatment, we observed using flow cytometry an increased macrophage infiltration with higher MHC II surface expression and increased phagocytic capacity in the TME of MC38-OVA tumours. These changes were not observed in tumours from *Adra2a*-KO mice (Fig. 4e and Extended Data Fig. 2d). Similar observations were made after GBZ treatment (Extended Data Fig. 6b), and also in the CT26 and TC-1 cancer models (Extended Data Fig. 6c,d). This modulation of macrophages by α2-AR agonists suggested that macrophages could be the primary cell compartment acted on by α2-AR agonists in mediating their anti-tumour effect.

To confirm their key role, we depleted macrophages in MC38-OVA tumour-bearing mice with clodronate liposomes, and we observed a reduced anti-tumour effect of CLD along with a lack of TIL increase (Fig. 4f and Extended Data Fig. 6e). Notably, PMN-MDSCs were also reduced after liposomal-clodronate treatment (Extended Data Fig. 6f). Furthermore, when we adoptively transferred WT macrophages into *Adra2a*-KO mice, we restored the anti-tumour effect of CLD and the TIL increase (Fig. 4g). We validated that adoptively transferred macrophages do migrate into tumours and lymph nodes (Extended Data Figs. 2e and 6g). These observations indicated the involvement of macrophages in the anti-tumour effect of α2-AR agonists.

Consistent with this, in vitro exposure of mouse macrophages to α2-AR agonists enhanced their ability to stimulate allogeneic $CD4^+$ and $CD8^+$ T cells (Extended Data Fig. 6h). Notably, while $CD4^+$ T cells were stimulated directly by CLD-treated macrophages, the increased proliferation of $CD8^+$ T cells required the presence of $CD4^+$ T cells in the co-culture (Extended Data Fig. 6h). Similarly, when we co-cultured ovalbumin-pulsed syngeneic macrophages with OVA-specific $CD4^+$ (OT-II) and $CD8^+$ (OT-I) T cells, we observed increased proliferation of both after CLD treatment (Extended Data Figs. 2h and 6i), and increased interferon-γ (IFNγ) production by OT-I $CD8^+$ T cells (Extended Data Figs. 2g and 6j). These effects were blocked by anti-MHC II antibodies and were absent in co-cultures with *Adra2a-KO* macrophages. In vivo, depletion of $CD4^+$ T cells in the TC-1 model abolished the anti-tumour effect of CLD (Extended Data Fig. 7a,b) and the increased $CD8^+$ T cell infiltration in the tumour and in secondary lymphoid organs (Extended Data Fig. 7c), further supporting the critical role of $CD4^+$ T cells in mediating the effects of α2-AR agonists. Similarly, the anti-tumour effect of CLD in both the TC-1 and the MC38-OVA models was attenuated in mice that were treated with MHC class II blocking antibodies (Extended Data Fig. 7d,e). These results are consistent with a model in which α2-AR agonists activate macrophages to stimulate $CD4^+$ T lymphocytes, which then further activate $CD8^+$ T lymphocytes. Consistent with this, single-cell analysis of TC-1 tumours from mice treated with CLD revealed a strong increase in $CD4^+$ T cells (Extended Data Fig. 5f).

α2-AR activation inhibits adenylate cyclase, resulting in decreased production of cAMP and reduced PKA activity. We confirmed reduced PKA activity in myeloid cells isolated from tumours and lymph nodes from mice treated with CLD (Extended Data Fig. 8a (left)). These cells also showed increased MHC II expression (Extended Data Fig. 8a (right)). Similarly, in vitro differentiated M1 macrophages exposed to CLD showed reduced cAMP levels (Extended Data Fig. 8b). They also showed reduced PKA activity and increased MHC II expression, both of which were not observed in *Adra2a*-KO macrophages (Extended Data Fig. 8c). However, it remains to be determined whether the anti-tumour effects of α2-AR agonists are mediated by the cAMP–PKA pathway, either entirely or partially, and which downstream pathways are involved.

Translational relevance

We further evaluated the translational relevance of our findings. On the basis of the clinical data from TCGA, a Kaplan–Meier survival analysis showed a significant association between high expression of α2-AR and a better overall survival and progression-free survival in patients with lung adenocarcinoma (Extended Data Fig. 9a). However, there were only modest positive correlations between α2-AR expression and multiple immunomodulatory molecules (Extended Data Fig. 9b). Note that α2-AR expression per se may not suffice to trigger signalling if there is no ligand. We therefore evaluated whether there is a link between α2-AR signalling in human tumours and response to immunotherapy. To do so, we established an α2-AR activation signature on the basis of our bulk mouse transcriptomics data. This signature consists of two components that are either upregulated (Post-Up) or downregulated (Post-Down) after α2-AR treatment (Extended Data Fig. 9c and Supplementary Table 2). We then queried the effect of these two signature sets (human orthologue genes) on the clinical response to anti-PD-1 or anti-PD-L1 immunotherapy using TIDE (Extended Data Fig. 9d). Notably, for anti-PD-L1 treatment in metastatic urothelial carcinoma[37], we observed a worse survival associated with a high expression of the downregulated set ($P = 2.67 \times 10^{-2}$) (Extended Data Fig. 9d (left)). High expression of the upregulated set was associated with better outcomes of anti-PD-1 therapy in a melanoma trial[38] ($P = 1.03 \times 10^{-2}$) (Extended Data Fig. 9d (right)). The α2-AR activation signature also correlated with macrophage infiltration, T cell infiltration, TCR richness and IFNγ response in all human tumours from the TCGA dataset (Extended Data Fig. 9e). These observations suggest that α2-AR signalling induces transcriptomic changes that correlate with a better response to immunotherapy. This further supports the translational potential of our findings.

Together, our results provide evidence that agonists of the α2-AR increase anti-tumour immune responses by modulating myeloid cells in the TME, and could be used for cancer immunotherapy. Notably, previous reports described increased proliferation of some tumour cell lines exposed to α2-AR agonists[39,40], whereas other reports found the opposite effects[41,42]. Moreover, in some in vivo experiments, treatment with α2-AR agonists favoured metastasis development[43,44]. The results that we report here in multiple tumour models, both in vitro and in vivo, do not confirm these early observations. One potential explanation for these divergent results is the dose—we used a dose of 5 mg per kg for the in vivo experiments, which is higher than the dose used in the previous studies (3–100 μg per kg). It is possible that the immune-mediated anti-tumour effects that we report here require such high doses and were therefore were not captured in the previous experiments. Indeed, the anti-tumour effect was not maintained when a tenfold reduced dose was used in daily intraperitoneal (i.p.) injections (Extended Data Fig. 1b). Notably, we observed a similar anti-tumour effect after delivery of CLD by the oral route in the drinking water as compared to daily i.p. injections (Extended Data Fig. 10a,b).

Discussion

The functional interplay between the autonomous nervous system and the immune system has been highlighted recently, particularly in the context of cancer[15,18,45–47]. In particular, modulation of anti-tumour immunity by the adrenergic system was reported for β2-adrenergic

signalling, which acts on several TME cell types to suppress immune responses[20,22,48]. Accordingly, β2-AR antagonists were found to potentiate ICB therapy, and are currently tested in clinical trials[23]. Here we show that the signal induced by α2-ARs is opposite, as their activation stimulates anti-tumour immunity. This is probably related to the opposite action of β2-ARs and α2-ARs on secondary signals. Although β2-ARs increase cAMP by activating adenylate cyclase through protein G_s, α2-ARs signal through the inhibitory protein G_i to inhibit adenylate cyclase and reduce cAMP levels. Previous research indicated that α-adrenergic signalling limited the development of MDSCs: chemical disruption of sympathetic signalling with a neurotoxin favoured MDSC development and suppressed anti-tumour immunity[47]. Our results are consistent with these observations, as we see a reduction in MDSCs in the TME after treatment with α2-AR agonists. We further highlight a direct effect of α2-AR agonists on macrophages, which appear to be their main cellular targets in the TME. As $CD4^+$ and $CD8^+$ T lymphocytes are required for the anti-tumour effect and are enriched in the TME after treatment, it appears that the α2-AR agonists activate macrophages to better recruit and activate $CD4^+$ and $CD8^+$ T lymphocytes in the TME. A schematic model of the anti-tumour effect of α2-AR agonists is shown in Extended Data Fig. 10c.

The relative role of macrophages and PMN-MDSCs in the anti-tumour effects of α2-AR agonists may vary according to the tumour model. In the TiRP model, we know from previous research that PMN-MDSCs are highly enriched and have a dominant suppressive role, by inducing TIL apoptosis through FasL[11]. Thus, the reduction in PMN-MDSC numbers probably has an important role to mediate the effects of α2-AR agonists in this model. However, macrophages may also contribute. In the MC38-OVA model, tumour-associated macrophages are highly abundant, and we observed marked phenotypic and transcriptomic changes in macrophages from treated MC38-OVA tumours, suggesting a prominent role of macrophages in this model. However, PMN-MDSCs were also reduced in numbers by CLD in MC38-OVA and MC38 tumours, and this probably also contributed to promoting tumour rejection by $CD8^+$ T lymphocytes. Besides MDSCs and macrophages, it is not impossible that α2-AR agonists also act on other cell types that contribute to their anti-tumour effects. Further work will be required to address this.

Importantly, we observed potent therapeutic efficacy of α2-AR agonists used as monotherapy in multiple tumour models, including humanized models and models that are totally resistant to current approaches of cancer immunotherapy. Such agonists have been used for decades in humans to treat high blood pressure. Their pharmacology and safety profile are well known. Despite the likely need to use higher doses than previously and to mitigate sedative effects, our findings warrant the clinical testing of α2-AR agonists in patients with cancer.

Online content

Any methods, additional references, Nature Portfolio reporting summaries, source data, extended data, supplementary information, acknowledgements, peer review information; details of author contributions and competing interests; and statements of data and code availability are available at https://doi.org/10.1038/s41586-023-06110-8.

1. Ribas, A. & Wolchok, J. D. Cancer immunotherapy using checkpoint blockade. *Science* **359**, 1350–1355 (2018).
2. Marin-Acevedo, J. A., Kimbrough, E. O. & Lou, Y. Next generation of immune checkpoint inhibitors and beyond. *J. Hematol. Oncol.* **14**, 45 (2021).
3. Rotte, A., Jin, J. Y. & Lemaire, V. Mechanistic overview of immune checkpoints to support the rational design of their combinations in cancer immunotherapy. *Ann. Oncol.* **29**, 71–83 (2018).
4. Giovannitti, J. A. Jr., Thoms, S. M. & Crawford, J. J. Alpha-2 adrenergic receptor agonists: a review of current clinical applications. *Anesth. Prog.* **62**, 31–39 (2015).
5. Kim, T. J., Sun, J., Lu, S., Zhang, J. & Wang, Y. The regulation of beta-adrenergic receptor-mediated PKA activation by substrate stiffness via microtubule dynamics in human MSCs. *Biomaterials* **35**, 8348–8356 (2014).
6. Sucharov, C. C., Dockstader, K., Nunley, K., McKinsey, T. A. & Bristow, M. β-Adrenergic receptor stimulation and activation of protein kinase A protect against α1-adrenergic-mediated phosphorylation of protein kinase D and histone deacetylase 5. *J. Card. Fail.* **17**, 592–600 (2011).
7. Wang, W. & Cao, X. β-Adrenergic signaling in tumor immunology and immunotherapy. *Crit. Rev. Immunol.* **39**, 93–103 (2019).
8. Allard, B., Allard, D., Buisseret, L. & Stagg, J. The adenosine pathway in immuno-oncology. *Nat. Rev. Clin. Oncol.* **17**, 611–629 (2020).
9. Ching, M. M., Reader, J. & Fulton, A. M. Eicosanoids in cancer: prostaglandin E2 receptor 4 in cancer therapeutics and immunotherapy. *Front. Pharmacol.* **11**, 819 (2020).
10. Huijbers, I. J. et al. An inducible mouse model of melanoma expressing a defined tumor antigen. *Cancer Res.* **66**, 3278–3286 (2006).
11. Zhu, J. et al. Resistance to cancer immunotherapy mediated by apoptosis of tumor-infiltrating lymphocytes. *Nat. Commun.* **8**, 1404 (2017).
12. Hennequart, M. et al. Constitutive IDO1 expression in human tumors is driven by cyclooxygenase-2 and mediates intrinsic immune resistance. *Cancer Immunol. Res.* **5**, 695–709 (2017).
13. Hedner, T. et al. Yohimbine pharmacokinetics and interaction with the sympathetic nervous system in normal volunteers. *Eur. J. Clin. Pharmacol.* **43**, 651–656 (1992).
14. Altman, J. D. et al. Abnormal regulation of the sympathetic nervous system in α_{2A}-adrenergic receptor knockout mice. *Mol. Pharmacol.* **56**, 154–161 (1999).
15. Godinho-Silva, C., Cardoso, F. & Veiga-Fernandes, H. Neuro-immune cell units: a new paradigm in physiology. *Ann. Rev. Immunol.* **37**, 19–46 (2019).
16. Starke, K., Endo, T. & Taube, H. D. Relative pre- and postsynaptic potencies of alpha-adrenoceptor agonists in the rabbit pulmonary artery. *Naunyn Schmiedebergs Arch. Pharmacol.* **291**, 55–78 (1975).
17. MacMillan, L. B., Hein, L., Smith, M. S., Piascik, M. T. & Limbird, L. E. Central hypotensive effects of the alpha2a-adrenergic receptor subtype. *Science* **273**, 801–803 (1996).
18. Zahalka, A. H. & Frenette, P. S. Nerves in cancer. *Nat. Rev. Cancer* **20**, 143–157 (2020).
19. Yang, J. H., Lee, E. O., Kim, S. E., Suh, Y. H. & Chong, Y. H. Norepinephrine differentially modulates the innate inflammatory response provoked by amyloid-β peptide via action at β-adrenoceptors and activation of cAMP/PKA pathway in human THP-1 macrophages. *Exp. Neurol.* **236**, 199–206 (2012).
20. Wu, J. J. et al. G protein-coupled receptor kinase 2 regulating β2-adrenergic receptor signaling in M2-polarized macrophages contributes to hepatocellular carcinoma progression. *Onco Targets Ther.* **12**, 5499–5513 (2019).
21. Qiao, G. et al. β-Adrenergic signaling blocks murine $CD8^+$ T-cell metabolic reprogramming during activation: a mechanism for immunosuppression by adrenergic stress. *Cancer Immunol. Immunother.* **68**, 11–22 (2019).
22. Mohammadpour, H. et al. β2 adrenergic receptor-mediated signaling regulates the immunosuppressive potential of myeloid-derived suppressor cells. *J. Clin. Invest.* **129**, 5537–5552 (2019).
23. Gandhi, S. et al. Phase I clinical trial of combination propranolol and pembrolizumab in locally advanced and metastatic melanoma: safety, tolerability, and preliminary evidence of antitumor activity. *Clin. Cancer Res.* **27**, 87–95 (2021).
24. Rohrer, D. K., Chruscinski, A., Schauble, E. H., Bernstein, D. & Kobilka, B. K. Cardiovascular and metabolic alterations in mice lacking both β1- and β2-adrenergic receptors. *J. Biol. Chem.* **274**, 16701–16708 (1999).
25. Kokolus, K. M. et al. Beta blocker use correlates with better overall survival in metastatic melanoma patients and improves the efficacy of immunotherapies in mice. *Oncoimmunology* **7**, e1405205 (2018).
26. Kim, R. et al. Ferroptosis of tumour neutrophils causes immune suppression in cancer. *Nature* **612**, 338–346 (2022).
27. Fukata, M. et al. Innate immune signaling by Toll-like receptor-4 (TLR4) shapes the inflammatory microenvironment in colitis-associated tumors. *Inflamm. Bowel Dis.* **15**, 997–1006 (2009).
28. Medzhitov, R. Toll-like receptors and innate immunity. *Nat. Rev. Immunol.* **1**, 135–145 (2001).
29. Park, L. et al. Innate immunity receptor CD36 promotes cerebral amyloid angiopathy. *Proc. Natl Acad. Sci. USA* **110**, 3089–3094 (2013).
30. McArdel, S. L., Terhorst, C. & Sharpe, A. H. Roles of CD48 in regulating immunity and tolerance. *Clin. Immunol.* **164**, 10–20 (2016).
31. Readinger, J. A., Mueller, K. L., Venegas, A. M., Horai, R. & Schwartzberg, P. L. Tec kinases regulate T-lymphocyte development and function: new insights into the roles of Itk and Rlk/Txk. *Immunol. Rev.* **228**, 93–114 (2009).
32. Ushio, A. et al. CCL22-producing resident macrophages enhance T cell response in Sjogren's syndrome. *Front. Immunol.* **9**, 2594 (2018).
33. Peng, S. L., Gerth, A. J., Ranger, A. M. & Glimcher, L. H. NFATc1 and NFATc2 together control both T and B cell activation and differentiation. *Immunity* **14**, 13–20 (2001).
34. Tsaytler, P., Harding, H. P., Ron, D. & Bertolotti, A. Selective inhibition of a regulatory subunit of protein phosphatase 1 restores proteostasis. *Science* **332**, 91–94 (2011).
35. Zhang, L. et al. Single-cell analyses inform mechanisms of myeloid-targeted therapies in colon cancer. *Cell* **181**, 442–459 (2020).
36. Voon, D. C., Hor, Y. T. & Ito, Y. The RUNX complex: reaching beyond haematopoiesis into immunity. *Immunology* **146**, 523–536 (2015).
37. Mariathasan, S. et al. TGFβ attenuates tumour response to PD-L1 blockade by contributing to exclusion of T cells. *Nature* **554**, 544–548 (2018).
38. Gide, T. N. et al. Distinct immune cell populations define response to anti-PD-1 monotherapy and anti-PD-1/anti-CTLA-4 combined therapy. *Cancer Cell* **35**, 238–255 (2019).
39. Castillo, L. F., Rivero, E. M., Goffin, V. & Luthy, I. A. $Alpha_2$-adrenoceptor agonists trigger prolactin signaling in breast cancer cells. *Cell. Signal.* **34**, 76–85 (2017).
40. Christensen, L. A., Finch, R. A., Booker, A. J. & Vasquez, K. M. Targeting oncogenes to improve breast cancer chemotherapy. *Cancer Res.* **66**, 4089–4094 (2006).
41. Kanno, N. et al. Stimulation of alpha2-adrenergic receptor inhibits cholangiocarcinoma growth through modulation of Raf-1 and B-Raf activities. *Hepatology* **35**, 1329–1340 (2002).
42. Maccari, S. et al. α-Adrenoceptor stimulation attenuates melanoma growth in mice. *Br. J. Pharmacol.* **179**, 1371–1383 (2022).

43. Szpunar, M. J., Burke, K. A., Dawes, R. P., Brown, E. B. & Madden, K. S. The antidepressant desipramine and α2-adrenergic receptor activation promote breast tumor progression in association with altered collagen structure. *Cancer Prev. Res.* **6**, 1262–1272 (2013).
44. Lavon, H. et al. Dexmedetomidine promotes metastasis in rodent models of breast, lung, and colon cancers. *Br. J. Anaesth.* **120**, 188–196 (2018).
45. Grebe, K. M. et al. Sympathetic nervous system control of anti-influenza CD8$^+$ T cell responses. *Proc. Natl Acad. Sci. USA* **106**, 5300–5305 (2009).
46. Eng, J. W. et al. A nervous tumor microenvironment: the impact of adrenergic stress on cancer cells, immunosuppression, and immunotherapeutic response. *Cancer Immunol. Immunother.* **63**, 1115–1128 (2014).
47. Nevin, J. T., Moussa, M., Corwin, W. L., Mandoiu, I. I. & Srivastava, P. K. Sympathetic nervous tone limits the development of myeloid-derived suppressor cells. *Sci. Immunol.* https://doi.org/10.1126/sciimmunol.aay9368 (2020).
48. Qiao, G. et al. Chronic adrenergic stress contributes to metabolic dysfunction and an exhausted phenotype in T cells in the tumor microenvironment. *Cancer Immunol. Res.* **9**, 651–664 (2021).

Methods

Mice

TiRP mice were created by crossing *Ink4a/Arf*$^{flox/flox}$ mice with mice carrying a transgenic construct controlled by the tyrosinase promoter and driving the expression of *H-Ras*^{12V} and *Trap1a*, which encodes a MAGE-type tumour antigen P1A; the promoter is separated from the coding region by a stop cassette made of a floxed self-deleting CreER[10]. Those mice were backcrossed to a B10.D2 background and bred to homozygosity. TCRP1A mice heterozygous for the H2L^{d}/P1A$_{35\text{-}43}$-specific TCR transgene were kept on the *B10.D2;Rag-1*$^{-/-}$ background[49]. NSG mice (strain *NOD.Cg-Prkdc*^{scid} *Il2rg*^{tm1Wjl}*/SzJ*), C57BL/6J mice and BALB/c mice were used in tumour transplantation experiments. *Adra2a*-KO mice (strain *B6.129-Adra2a*$^{tm1Bkk/J}$, 004367) were obtained from Jackson Laboratory and genotyped as described previously[50], using the following primers (5′-GGTGACACTGA CGCTGGTTT (forward), 5′-AAGGAGATGACAGCCGAGAT (reverse WT) and 5′-CGAGATCCACTAGTTCTAGC (reverse KO)). *Adrb1/b2*-KO mice (strain *Adrb1*^{tm1Bkk}*;Adrb2*$^{tm1Bkk/J}$, 003810) were obtained from Jackson Laboratory, backcrossed with C57BL/6J mice and genotyped using the standard protocol provided by Jackson Laboratory. OT-I mice (C57BL/6-Tg(TcraTcrb)1100Mjb/Crl) and OT-II mice (C57BL/6-Tg(TcraTcrb)425Cbn/Crl) were obtained from Charles River. Ly5.1 Mice were obtained from Charles River. All mice used were age matched and were assigned randomly to experimental and control groups. Investigators were blinded to allocation during experiments. Female TiRP mice (aged 10–18 weeks), NSG mice (aged 8–14 weeks), and C57BL/6J, BALB/c, *Adra2a*-KO and *Adrb1/b2*-KO mice (aged 6–12 weeks) were used for experiments on antitumour effect in vivo. Female TCR-P1A, TCR-OT I and TCR-OT II mice (aged 9–12 weeks) were used for CD8 T cell isolation. Female Ly5.1 mice (aged 6–12 weeks) were used to differentiate macrophages in vitro for adoptive cell transfer. Female and male DBA/2 mice (aged 6–12 weeks) were used for CD8 and CD4 T cell isolation for in vitro assays. The sample size was chosen on the basis of preliminary experiments and previously published results. All mice used in this study were produced under specific-pathogen-free conditions at the animal facility of the de Duve Institute, housed at an ambient temperature of around 21–23 °C under a humidity of 40–60% and a light–dark cycle of 12 h–12 h. All of the rules concerning animal welfare were respected according to the 2010/63/EU Directive. All of the procedures were performed with the approval of the Animal Ethical Committee of UCLouvain university, with reference 2015/UCL/MD/14 and 2019/UCL/MD/019.

Cell lines

CT26, B16F1, HEPA1-6, J558, 4T1, Renca and PC-3 cells were purchased from the American Type Culture Collection (ATCC). The B16F10-OVA cell line was generated by transduction of B16F10 cells (ATCC) with a lentivirus encoding chicken ovalbumin protein in the laboratory. The E.G7-OVA cell line was provided by J. Vanginderachter. The TS/A cell line was provided by G. Prodi. The LS411N cell line was provided by N. Odartchenko. The T429.6 cell line was generated from the induced TiRP melanoma tumour model in the laboratory[11]. The MC38 cell line was provided by M. Waldner. The MC38-OVA cell line was generated by transduction of MC38 cells with lentivirus encoding chicken ovalbumin protein. The SK-OV-3 cell line was purchased from Cell Line Service. The TC-1 cell line was provided by C. Gérard. The CMS5a cell line was obtained from the laboratory of H. Shiku. All tumour cell lines were tested regularly for mycoplasma contamination using the MycoAlert Mycoplasma Detection Kit (LT07-318, Lonza) and were verified to be negative before using for different assays and studies. All mouse tumour cell lines were validated using the ATCC STR profiling Cell Authentication Service. All human cell lines were validated using the Eurofin Cell line Authentication Service by PCR single-locus technology.

Cell culture

L1210.P1A.B7-1 cells were cultured in Dulbecco's modified Eagle medium (DMEM) (31885023, Gibco, Thermo Fisher Scientific) supplemented with 10% fetal bovine serum (FBS) (F7524, Sigma Life Science), penicillin (100 U ml^{-1}) and streptomycin (100 µg ml^{-1}).

Mouse TCRP1A and TCROVA CD8^{+} T cells were cultured in IMDM medium (21980032, Gibco, Thermo Fisher Scientific) supplemented with 10% FBS (F7524, Sigma Life Science), penicillin (100 U ml^{-1}), streptomycin (100 µg ml^{-1}), a mix of amino acids (L-asparagine (0.24 mM), L-arginine (0.55 mM) and L-glutamine (1.5 mM)) and recombinant IL-2 (25 U ml^{-1}) (PROLEUKIN, Novartis). Cells were maintained at 37 °C under an atmosphere containing 8% CO_2. CT26, B16F1, B16F10-OVA, MC38, MC38-OVA, Hepa 1-6, TC-1, J558, TS/A, CMS5a, SK-OV-3, LS411N and PC-3 cells were cultured in IMDM medium (21980032, Gibco, Thermo Fisher Scientific) supplemented with 10% FBS (F7524, Sigma Life Science), penicillin (100 U ml^{-1}), streptomycin (100 µg ml^{-1}), a mix of amino acids (L-asparagine (0.24 mM), L-arginine (0.55 mM) and L-glutamine (1.5 mM)). Renca cells were cultured in the same medium further supplemented with 1 mM pyruvate (11360070, Gibco, Thermo Fisher Scientific). E.G7-OVA and 4T1 cells were cultured in RPMI medium (52400025, Gibco, Thermo Fisher Scientific) supplemented with 10% FBS (F7524, Sigma Life Science), penicillin (100 U ml^{-1}), streptomycin (100 µg ml^{-1}) and a mix of amino acids (L-asparagine (0.24 mM), L-arginine (0.55 mM) and L-glutamine (1.5 mM)). All cells were maintained at 37 °C under an atmosphere containing 8% CO_2.

Drug administration

Mice received a daily i.p. injection of GBZ (5 mg per kg), CLD (5 mg per kg), GFC (2 mg per kg), YHB (5 mg per kg), PHE (5 mg per kg), PRP (5 mg per kg) or vehicle (PBS) from the day of randomization until the day of euthanasia. Mice (particularly BALB/c mice) were strongly sedated after injection of α2-AR agonists, but they always fully recovered after 30–60 min. Furthermore, α2-AR agonists increased the aggressiveness of male mice; therefore, female mice were used for all experiments. For the co-administration of adrenergic receptor agonist and antagonist, mice received daily injections of vehicle control, GBZ (5 mg per kg, i.p.) or GBZ (5 mg per kg, i.p.) plus YHB (10 mg per kg, i.p.), CLD (5 mg per kg, i.p.) or CLD (5 mg per kg, i.p.) plus YHB (10 mg per kg, i.p.) when the tumour size was around 50 mm^3, until the day of euthanasia. When given in drinking water, CLD was diluted in sterilized water at a concentration of 10 µg per ml.

The anti-CTLA4 (BioXcell, 9H10, 40 µg per mouse) and anti-PD-1 (BioXcell, RMP1-14, 200 µg per mouse) antibodies were injected twice per week i.p. starting 1 day before the α2-AR agonist injections. The anti-MHC II antibody (BioXcell, Y-3P, 500 µg per mouse) was injected twice per week i.p. starting 1 day before the α2-AR agonist injections. The corresponding isotype controls were injected accordingly (InVivoMAb rat IgG2b isotype control (BE0090, BioXcell) InVivoMAb rat IgG2a isotype control (BE0089, BioXcell), InVivoMAb polyclonal Syrian hamster IgG (BE0087, BioXcell)). One day before the initiation of the therapy regimens, fingolimod (FTY720, Enzo Life Sciences) was given to the mice to inhibit lymphocyte migration out of the lymphoid organs. Mice received a dose of 10 µg FTY720 per mouse i.p. daily throughout the experiment.

MDSC suppression assay

After mechanical and enzymatic dissociation of induced TiRP tumours, Ly6G^{high} cells were further purified by magnetic sorting (Miltenyi) and confirmed as PMN-MDSC by fluorescence-activated cell sorting (FACS) analysis (Gr-1^{high}CD11b^{+}Ly6C^{low}Ly6G^{high}). TCRP1A CD8^{+} T cells activated in vitro for 4 days with irradiated (100 Gy) L1210.P1A.B7-1 cells were purified, washed, counted and 2×10^5 viable cells were seeded in a 96-well plate in IMDM complete medium. TCRP1A CD8^{+} T cells were co-cultured with Ly6G^{+} MDSCs at the indicated ratios for 2 days at 37 °C.

T cell apoptosis was assessed by annexin V staining. T cell number was counted by flow cytometry analysis using Precision count beads.

In vitro T cell activity assay

TCRP1A $CD8^+$ T cells activated in vitro for 4 days with irradiated L1210.P1A.B7-1 cells were purified, washed, counted and 2×10^5 viable cells were seeded in a 96-well plate in IMDM complete medium. T cell degranulation was induced by co-culturing the $CD8^+$ T cells with L1210.P1A.B7-1 cells with and without CLD. After 2 h of co-culture, T cell degranulation was measured by examination of LAMP1 expression. For assessing the IFNγ production, TCRP1A $CD8^+$ T cells were co-cultured with L1210.P1A.B7-1 cells for 16 h with and without CLD, the supernatant was collected and the amount of secreted IFNγ was quantified by ELISA according to the manufacturer's instruction (DY485, R&D systems). In parallel, T cells were also counted at the end of the 16 h co-culture.

Tumour induction with 4-OH-tamoxifen

A fresh solution of 4-OH-tamoxifen was prepared by dissolving 4-OH-tamoxifen (Imaginechem) in 100% ethanol and mineral oil (ratio 1:9) followed by 30 min sonication, and injected subcutaneously (2 mg per 200 µl per mouse) into the neck area of sex-matched 7-week-old TiRP mice.

Tumour transplantation

Different tumour cell lines were cultured at 37 °C in an atmosphere containing 8% CO_2. Cells were collected and injected (1 million cells) subcutaneously into the right flank of the recipient mice.

Adoptive cell transfer of $CD8^+$ T cells

For the adoptive cell transfer (ACT), P1A-specific (TCRP1A) $CD8^+$ T cells or OVA-specific (TCROVA) $CD8^+$ T cells were isolated from the spleens and lymph nodes of TCRP1A mice or OT-I mice, respectively. TCRP1A $CD8^+$ T cells were stimulated in vitro by co-culture with irradiated (100 Gy) L1210.P1A.B7-1 cells[51] at a 1:2 ratio (0.5×10^5 $CD8^+$ T cells and 10^5 L1210.P1A.B7-1 cells per well in 48-well plates) in IMDM (GIBCO) containing 10% fetal bovine serum supplemented with L-arginine (0.55 mM, Merck), L-asparagine (0.24 mM, Merck), glutamine (1.5 mM, Merck), β-mercaptoethanol (50 µM, Sigma-Aldrich), 50 U ml^{-1} penicillin and 50 µg ml^{-1} streptomycin (Life Technologies). TCROVA $CD8^+$ T cells were stimulated in vitro with Mouse T-Activator CD3/CD28 Dynabeads (11453D, Gibco, Thermo Fisher Scientific) in a 48-well plate (3548, Corning Incorporated) at a ratio of 1 to 1 (100,000 TCROVA $CD8^+$ T cells mixed with 100,000 beads per well) in the presence of 25 U ml^{-1} interleukin-2. Then, 4 days after T cell activation, TCRP1A $CD8^+$ T cells were purified on a Lymphoprep gradient (StemCell) and 10^7 living cells were injected intravenously in 200 µl PBS into TiRP-tumour bearing mice on the day of randomization. For TCROVA $CD8^+$ T cells, cells were collected 7 days after activation and 10^7 living cells were injected intravenously in 200 µl PBS into mice bearing MC38-OVA tumours.

Adoptive cell transfer with in vitro differentiated macrophages

Femora and tibiae of 8–10-week-old C57BL/6J mice were flushed with DMEM medium. Bone marrow cells were cultured in DMEM medium containing 10% FBS, 10 ng ml^{-1} MCSF, 50 U ml^{-1} penicillin and 50 µg ml^{-1} streptomycin (Life Technologies) in an atmosphere of 37 °C, 5% CO_2. The medium was refreshed on day 4. On day 7, the medium was replaced by DMEM medium containing 10 ng ml^{-1} IFNγ, 10% FBS, 10 ng ml^{-1} MCSF, 50 U ml^{-1} penicillin and 50 µg ml^{-1} streptomycin (Life Technologies) to differentiate macrophages, and the cells were further cultured for another 3 days. On day 10, differentiated macrophages were detached from the culture flask using Accutase (00-4555-56, Gibco, Thermo Fisher Scientific), resuspended in PBS and transferred to recipient mice by intravenous injection (2×10^6 cells per mouse) when the tumour size reached around 100 mm^3. Mice then received daily CLD treatment (i.p., 5 mg per kg) starting 1 day after macrophage transfer. In the experiment in which $CD45.1^+$ macrophages were used for adoptive cell transfer, bone marrow cells from Ly5.1 C57BL/6J congenic mice expressing the CD45.1 allele were used for macrophage differentiation.

Tumour growth measurement

The size of individual tumours was measured every 2 or 3 days. The tumour diameters (width, length) were measured using digital callipers. Tumour volumes were calculated using the following formula: volume = (width^2 × length)/2. Tumour measurement was recorded and calculated using Microsoft Excel for Mac (v.16.7).

Isolation of human PBMCs

PBMCs were derived from the blood of different patients with haemochromatosis, courtesy of Saint-Luc University Hospital. They were isolated by centrifugation on a Lymphoprep gradient and were used freshly for adoptive cell transfer. The study protocol was approved by the UCLouvain commission d'éthique hospitalo-facultaire under authorization approval no. CEHF 2021/13SEP/373. The ethical approval encompasses an exemption of informed consent based on the fact that we use only blood that qualifies as 'residual human body material', which needs to be collected as a therapeutic measure for patients with haemochromatosis. The option to not opt out was checked for all patients.

Human xenografts in NSG mice reconstituted with human lymphocytes

NSG mice (from The Jackson Laboratory) were bred at the animal facility of the de Duve Institute. Handling of mice and experimental procedures were conducted in accordance with national and institutional guidelines for animal care. NSG mice were injected subcutaneously with 1.5×10^6 SK-OV-3, LS411N or PC-3 cells. After tumour appearance, tumours were measured, mice were randomized on the basis of tumour size and injected or not with 3×10^6 human allogeneic HLA-mismatched PBMCs (PBMC; d0) intravenously. Guanabenz or CLD (5 mg per kg) was injected i.p. daily. Tumours were measured at regular intervals with electronic callipers.

Single-cell preparation for FACS staining

Tumours and spleens were isolated from tumour-bearing mice. Tumour samples were dissociated using a cocktail of three enzymes (collagenase I, collagenase II and dispase) with the help of a gentleMACS dissociator (Miltenyi). The spleens were gently smashed in cell culture medium to generate a cell suspension. Single cells were obtained by filtration of tissue homogenate through a 40 µm filter.

Generation of *Adra2a*-KO tumour cells

TC-1 tumour cells were electroporated with Cas9/gRNA RNP targeting *Adra2a* (Mm. Cas9.ADRA2A.1AA, Mm. Cas9.ADRA2A.1AB, IDT). Cells were resuspended in SE Cell Line 4D-Nucleofector X Kit solution with supplement (Lonza), transferred to 16-well Nucleocuvette strips and electroporated using the program DS-120. Then, 1 week after electroporation, single-cell clones were isolated by FACS sorting (MA900 Multi-Application Cell Sorter) and were expanded and validated using RT–qPCR analysis.

CFSE tumour proliferation assay

Carboxyfluorescein diacetate succinimidyl ester (CFDA-SE, C1157, Molecular Probes) stock solution (5 mM) was dissolved in DMSO. A total of 2×10^7 tumour cells in 10 ml IMDM medium without serum was mixed with 2.5 µM CFDA-SE, and the cell–CFDA-SE mixture was incubated at 37 °C for 10 min. The labelling reaction was stopped by incubation with full IMDM medium containing serum. The CFSE-labelled cells were washed twice with IMDM medium containing 10% FBS and recounted, then used for proliferation assessment. The CFSE fluorescence intensity was measured using flow cytometry analysis.

MTT assay

Tumour cells (1.5×10^3) were plated in triplicate in a 96-well plate in a cell–cell direct-contact manner with 0.1 ml complete medium containing different α2-AR agonists at different concentrations. Then, 48 h after treatment, cell viability was measured using the MTT (3-(4,5-dimethyl-thiazol-2-yl)-2,5-diphenyltetrazolium bromide) assay.

Western blot analysis

Cell lysates were added with Pierce Lane Marker Reducing Sample Buffer (Thermo Fisher Scientific, 39000), heated (95 °C, 10 min) and loaded onto a polyacrylamide gel (Bolt 4–12%, Invitrogen, NW04122). After migration, proteins were transferred to iBlot NC stacks (Invitrogen, IB23002). The membrane was blocked with 5% BSA and stained with anti-phosphorylated CREB (Ser133) (Cell Signaling, 87G3, 9198, 1:1,000), CREB (Cell Signaling, 48H2, 9197, 1:1,000) or anti-β-actin (Cell Signaling, 13E5, 5125, 1:1,000) antibodies. The secondary antibodies used were anti-rabbit IgG HRP (Cell Signaling, 7074, 1:2,500). Protein detection was performed using the chemiluminescent SuperSignal WestPico substrate (Thermo Fisher Scientific, 34578). Pictures were captured using the Fusion FX camera (Vilbert Lourmat).

Macrophage co-culture assay

M1 Macrophages were differentiated in vitro as described above. For co-culture experiments with allogeneic T cells, 3×10^4 naive mouse $CD4^+$ and/or $CD8^+$ T cells were co-cultured with 5×10^4 allogeneic M1 macrophages per 200 µl in round-bottom 96-well culture plates in the presence of the indicated concentrations of CLD. Then, 4 days after co-culture, T cell numbers were recorded by flow cytometry analysis using Precision count beads.

For co-culture experiments with syngeneic OT-I $CD8^+$ T cells and OT-II $CD4^+$ T cells, 3×10^4 CFSE labelled naive mouse $CD4^+$ and/or $CD8^+$ T cells were co-cultured with 5×10^4 M1 macrophages with or without 2.5 µM CLD in presence of 1 µg ml^{-1} ovalbumin protein (InvivoGen, vac-pova-25) per 200 µl in round-bottom 96-well culture plates in the presence of 2.5 µM of CLD. To assess the role of MHC II, anti-MHC II antibodies (50 µg ml^{-1}) were added in the co-culture as indicated. Then, 3 days after co-culture, the T cell proliferation index was analysed by flow cytometry analysis using the function of proliferation modelling. IFNγ production was assessed in OT-I $CD8^+$ T cells co-cultured as described above and stimulated with 3×10^4 E.G7-OVA tumour cells for 16 h. Intracellular IFNγ was measured by flow cytometry.

cAMP quantification

In vitro differentiated M1 macrophages were treated with different concentrations of CLD. The Cyclic AMP Competitive ELISA Kit was used to assay cAMP (EMSCAMPL, Thermo Fisher Scientific).

FACS staining of tumour-infiltrating immune cells

Single-cell suspensions from tumours and spleens of tumour-bearing mice were counted and plated in round-bottom 96-well plates (353910, Falcon) at a density of 10^6 cells per well. Cells were blocked with Mouse TruStain FcX and were stained with the viability dye Efluor 780 (65-0865-14, Invitrogen, 1 in 500 dilution in PBS) to identify living cells, followed by staining with P1A-tetramer (home-made H-2-L^d folded with P1A peptide LPYLGWLVF; 1 in 50 dilution) and anti-CD45 and anti-CD8 antibodies to identify tumour-infiltrating $CD8^+$ T cells. The apoptosis of T cells was analysed using annexin V-APC. Ly6C-PerCP, Gr-1-APC, Ly6G-Bv510 and CD11b-Bv711 antibodies were used to identify MDSCs. F4/80-PE, MHC class II-APC (1:500) and CD11c-Bv421 antibodies were used to identify macrophages. PD-1-FITC, PD-L1-PE, IFNγ-APC and TNF-Bv711 were used to evaluate the expression of different immune modulators by cells of the TME. All antibodies were used at a dilution of 1:200 unless otherwise specified. For intracellular staining, cells were fixed using fixation buffer (BioLegend, 420801) and permeabilized with perm/wash permeabilization buffer (BioLegend, 421002). Antibodies were purchased from BioLegend and the concentration of antibodies was used according to the manufacturer's recommendations. Phagocytosis of macrophages was measured using pHrodo Red E. coli BioParticles Conjugates for Phagocytosis (Thermo Fisher Scientific) according to the manufacturer's recommendations. Flow cytometry data were analysed using Flowjo (v.10.7.2).

In vivo depletion of $CD8^+$ or $CD4^+$ T cells

For CD8 T cell depletion, mice were given 500 µg of monoclonal antibody 53-6.7 (BioXCell) or normal rat IgG (controls) by the i.p. route 1 day before starting CLD treatment, and then 150 µg weekly. For CD4 T cell depletion, mice were given 500 µg of Ultra-LEAF Purified anti-mouse CD4 antibody (GK1.5, BioLegend) or normal rat IgG2b (controls) by the i.p. route 1 day before starting CLD treatment, and then 250 µg weekly. Depletion was checked by FACS at the end of the experiment.

In vivo depletion of macrophages

Clodronate liposomes and control liposomes were purchased from FormuMax Scientific, and were injected (150 µl of 7 mg ml^{-1}) i.p. 48 h before starting CLDtreatment, and repeated every 3 days until the end of the experiment. Depletion was checked by FACS at the end of the experiment.

RT–qPCR

The NucleoSpin RNA XS isolation kit (Macherey-Nagel) or NucleoSpin RNA isolation kit (Macherey-Nagel) was used to extract total RNA from cell lines or tumour tissues, respectively. RNA concentration was measured using the NanoDrop 2000c (Thermo Fisher Scientific). Reverse transcription was performed using the RevertAid RT kit (K1691, Thermo Fisher Scientific). qPCR reactions were performed with primers and probes specific for mouse *Adra2a* (Mm.PT.58.33590743.g), *Adra2b* (Mm.PT.58.6098909.g), *Adra2c* (Mm.PT.58.30363072.g), *Ifnb1* (Mm.PT.58.30132453.g), *Cxcl13* (Mm.PT.58.31389616), *Tlr1* (Mm.PT.58.45864869), *Tlr8* (Mm.PT.58.16021150), *Tlr7* (Mm.PT.58.10526075) and *Gapdh* (Mm.PT.39a.1) (housekeeping gene), and for human *ADRA2A* (Hs.PT.56a.878688.g), *ADRA2B* (Hs.PT.58.723437.g) and *GAPDH* (Hs.PT.39a.22214836) (housekeeping gene), using the Takyon ROX Probe 2× MasterMix dTTP Blue (UF-RPMT-B0701, Eurogentec) qPCR kit, and analysed on the Applied Biosystems StepOnePlus Real-Time PCR System (4376599, Thermo Fisher Scientific). All primers and probes were purchased from Integrated DNA Technologies. cDNA was amplified as follows: 45 cycles of a two-step PCR program at 95 °C for 3 s and 60 °C for 30 s. All determinations were performed in duplicates.

RNA-seq sample preparation

Total RNA was extracted from three PBS-treated MC38-OVA tumours, three CLD-treated and three GBZ-treated MC38-OVA tumours from WT mice or *Adra2a*-KO mice, 7 days after starting the treatment. Tumour tissue was collected and snap-frozen in liquid nitrogen. RNA extraction was initiated by grinding the tissue under liquid nitrogen into powder and further processed using the NucleoSpin RNA isolation kit (Macherey-Nagel). RNA quality was assessed using the Agilent 2100 Bioanalyzer System. RNA samples with an RNA integrity number above 7 were further used for RNA-seq. Strand-specific mRNA-seq libraries for the Illumina platform were generated and sequenced at Genewiz (BaseClear). Libraries were multiplexed, clustered and sequenced on the Illumina NovaSeq 6000, with paired-end 150 bp reads.

RNA-seq downstream analysis

Quality control and filtering was performed according to the trim galore! 0.6.5 protocol, which uses FastQC for quality control and Cutadapt for adapter trimming. Processed paired FASTQ files were mapped to the mouse reference GRCm38(Ensembl 96) and quantified using Kallisto (v.0.46.1)[52] on Ubuntu (v.20.04.1). The resulting transcript

abundance matrices (estimated counts) per sample were subsequently imported with tximport[53] (v.1.20.0) in R (v.4.0.3), summarized to gene level with TxDB (v.3.10) annotations and finally submitted for differential expression analysis with DESeq2[54] (v.1.32.0). Effect sizes for comparison between treated and untreated conditions were estimated using apeglm as implemented in DESeq2.

Gene-level expression data generated in this study for each of the conditions was L1-normalized per sample using scikit-learn[55] (v.0.24.1). Signature correlations between all samples were calculated as Spearman correlations (SciPy; v.1.6.2) using only the genes in the α2-AR activation signature. The resulting distance matrix was then projected on top of a manifold using UMAP-learn (v.0.5.1)[56]. Hierarchical clustering (SciPy; v.1.6.2) using Spearman correlation on the expression matrix of the α2-AR activation signature genes identified three broad clusters separating KO and unstimulated conditions from the stimulated WT samples, highlighted in Extended Data Fig. 4h with ellipses.

TCGA-based validation

Gene expression data and immune features associated with TCGA, as calculated previously[57] were downloaded from the corresponding GDC portal (https://gdc.cancer.gov/about-data/publications/panimmune; n = 10,496, 33 cancer types). H&E-derived metrics[58] for $CD8^+$ T cell infiltration were also obtained from the GDC (https://gdc.cancer.gov/about-data/publications/tilmap). Correlations between expression of a selected set of immune modulators and the ADRA2 metagene (sum of *ADRA2A, ADRA2B, ADRA2C*) were calculated using Spearman correlations with SciPy (v.1.6.2)[59]. Heat maps and box plots were plotted using Python (v.3.8.8), through matplotlib (v.3.5.2)[60] and seaborn (v.0.11.1)[61]. Kaplan–Meier curves based on gene expression were generated with lifelines (v.0.26.3), using the median gene expression as threshold between groups.

TIDE survival analysis

To test the survival impact of the up- and downregulation signatures, we consulted the TIDE[62] database through its web portal (http://tide.dfci.harvard.edu/login/). Gene signatures were entered as biomarker and tested for survival impact. Kaplan–Meier curves were calculated using the median value of the signature metagene to discriminate between high and low expression. Statistical significance was tested using two-sided Wald's tests in a Cox Proportional Hazards regression model.

Sample preparation for single-cell sequencing

MC38-OVA tumour samples isolated from mice treated with PBS or CLD (7 days after starting of the treatment) were pooled (10 mice per group) and dissociated using a cocktail of three enzymes (collagenase I, collagenase II and dispase) with the help of a gentleMACS dissociator (Miltenyi). The cell suspension was collected, filtered through a 70 µm filter (352350, FALCON) and washed with cold sterile PBS. Dead cell removal was performed using Ficoll gradient. In brief, cell pellets were resuspended in 10 ml PBS and gently layered on top of 10 ml density gradient medium (Lymphoprep) followed by a centrifugation at 3,000 rpm for 10 min at room temperature with the brake off. Cells were collected at the interface and prepared for single-cell sequencing as described by the manufacturer (10x Genomics) in the 'Methanol fixation of cells for single-cell RNA sequencing protocol'. Single-cell mRNA sequencing was performed at Single Cell Discoveries (single-cell sequencing service) according to standard 10x Genomics 3′ V3.1 chemistry. Before loading the cells onto the 10x Chromium controller, cells were rehydrated in rehydration buffer according to the vendor instructions. Cells were then filtered to prevent clumping and counted to assess cell integrity and concentration. Cells were loaded and the resulting sequencing libraries were prepared according to the standard 10x Genomics protocol. The DNA libraries were paired-end sequenced on the Illumina NovaSeq S4 system with a 2 × 150 bp Illumina kit. BCL files resulting from sequencing were transformed to FASTQ files with 10x Genomics Cell Ranger (v.6.1.2) mkfastq. FASTQ files were mapped using Cell Ranger count. During sequencing, read 1 was assigned 28 bp, and was used for identification of the Illumina library barcode, cell barcode and UMI. Read 2 was used to map to the reference transcriptome mm10 2020A. Filtering of empty barcodes was performed using Cell Ranger. Unsupervised clustering and differential gene expression analysis was performed using the Seurat1 R toolkit[63] (v.4.0.3). For TC-1 tumours, sample preparation was performed the same way as described above, except fresh cells were directly loaded, and the resulting sequencing libraries were prepared according to the standard 10x Genomics protocol.

scRNA-seq analyses

10x files generated by CellRanger (v.6.1.2) were loaded into Scanpy[64] (v.1.7.0) and quality-control metrics were calculated. Cells with either a low (<200) or higher than expected (>2,500) number of individual genes expressed were removed. Genes with very limited expression (less than 10 cells) were removed. Counts were normalized per 10,000 reads and $\log_2$-transformed. Differences in total counts per cell and mitochondrial content were regressed out. Highly variable genes were detected using the Seurat approach, with a mean expression cut-off of 0.125. Only highly variable genes were used for principal component analysis (PCA), clustering and downstream set enrichment analysis. We clustered MC38-OVA cells into groups with PhenoGraph (v.1.5.7)[65] (https://github.com/dpeerlab/phenograph) using the Leiden clustering algorithm. The parameters were k = 25, 5,000 iterations and random seed 770. The number of PCA components we selected explained 20% of the total variance in the dataset (n_comps=26). MC38-OVA cell populations were manually annotated per cluster on the basis of known marker genes (Supplementary File 1). In total, 12,066 MC38-OVA cells passed quality-control filtering. A total of 2,213 genes was identified as highly variable. Differential expression testing between treated and untreated was performed using Wilcoxon rank-sum tests with $\alpha = 0.05$, using Diffxpy (v.0.7.4). Analysis of ligand–receptor interactions between cells in the sample was performed with CellPhoneDB[66] (v.2.1.4). To this end, mouse genes were mapped to their human orthologues using BioMart (Ensembl release 104).

10x files generated by CellRanger for the TC-1 lung carcinoma validation set were loaded into R (v.4.2.0, patched, 2022-05-13 r82357) using the read10xCounts() function from the DropletUtils[67] package (v.1.16.0). Quality metrics were computed using the scuttle package[68] (v.1.6.3) and cells with over 10% of mitochondrial gene counts were removed. Counts were then normalized by deconvolution using the scran package[69] (v.1.24.1), and the 1,000 most variable genes were selected on the basis of their per-gene variance as implemented in scran. A total of 19,069 cells and the 1,000 most variable genes were used for downstream clustering and cell annotations. Clusters were identified using scran's clusterCells() function applying a two-step procedure, starting with a vector quantisation with k-means on the PCA-reduced data (200 centres and 100 iterations) to obtain representative centroids that were then subjected to nearest-neighbour graph-based clustering as described above, using $k = 10$ nearest neighbours. Cell type annotation was performed using the SingleR package (v.1.10.0) as described above, using the MC38-OVA colon carcinoma single-cell data annotations described above.

Set enrichment analysis

For both RNA-seq and scRNA-seq data, genes were pre-ranked on the basis of $\log_2$-transformed fold change and processed using GSEApy (v.0.10.5)[70], which implements the classical GSEA[71] analysis. Gene sets for mouse enrichment were obtained from http://baderlab.org/GeneSets on 2 November 2021.

Statistics

Statistical significance was assessed using two-sided unpaired Welch t-tests unless otherwise specified. P values are denoted by asterisks:

*$P < 0.05$, **$P < 0.01$, ***$P < 0.005$, ****$P < 0.0001$. For the mouse in vivo experiments, statistical significance was determined using two-way ANOVA to compare differences among multiple groups. All statistical analyses were performed using GraphPad Prism (v.8.4.3) for Mac (GraphPad Software; www.graphpad.com), R (v.4.0.3; for RNA-seq analysis) and R (v.4.2.0; for scRNA-seq analysis), and Python (v.3.7.3; for the RNA-seq and scRNA-seq data analysis) and Python (v.3.8.8; for data visualization).

Reporting summary

Further information on research design is available in the Nature Portfolio Reporting Summary linked to this article.

Data availability

All data supporting the findings of this study are available within the Article and its Supplementary Information. scRNA-seq and RNA-seq data were obtained from in-house experiments. Raw and processed data are available from the Gene Expression Omnibus under accession codes GSE227601 and GSE226290, respectively. Intermediate processed results have been archived at Zenodo DOIs https://doi.org/10.5281/zenodo.7751788 and https://doi.org/10.5281/zenodo.7789646. Source data are provided with this paper.

Code availability

Supporting R and Python scripts, with installation instructions and version numbers, are publicly available at GitHub (https://github.com/BVDElab/Tumour_immune_rejection) and archived at Zenodo. Code to generate the corresponding analyses or figures is available at https://doi.org/10.5281/zenodo.7751788 for Figs. 3i–j, 4a–d and Extended Data Fig. 5f; and at https://doi.org/10.5281/zenodo.7789646 for Extended Data Figs. 4h and 9c.

49. Shanker, A. et al. Thymocyte-intrinsic genetic factors influence CD8 T cell lineage commitment and affect selection of a tumor-reactive TCR. *J. Immunol.* **172**, 5069–5077 (2004).
50. Ohshima, M., Itami, C. & Kimura, F. The α2A-adrenoceptor suppresses excitatory synaptic transmission to both excitatory and inhibitory neurons in layer 4 barrel cortex. *J. Physiol.* **595**, 6923–6937 (2017).
51. Gajewski, T. F., Renauld, J. C., Van Pel, A. & Boon, T. Costimulation with B7-1, IL-6, and IL-12 is sufficient for primary generation of murine antitumor cytolytic T lymphocytes in vitro. *J. Immunol.* **154**, 5637–5648 (1995).
52. Bray, N. L., Pimentel, H., Melsted, P. & Pachter, L. Near-optimal probabilistic RNA-seq quantification. *Nat. Biotechnol.* **34**, 525–527 (2016).
53. Soneson, C., Love, M. I. & Robinson, M. D. Differential analyses for RNA-seq: transcript-level estimates improve gene-level inferences. *F1000Res* **4**, 1521 (2015).
54. Love, M. I., Huber, W. & Anders, S. Moderated estimation of fold change and dispersion for RNA-seq data with DESeq2. *Genome Biol.* **15**, 550 (2014).
55. Pedregosa, F. et al. Scikit-learn: Machine Learning in Python. Journal of Machine Learning Research 12; 2825-2830 (2011).
56. Sainburg, T., McInnes, L. & Gentner, T. Q. Parametric UMAP embeddings for representation and semisupervised learning. *Neural Comput.* **33**, 2881–2907 (2021).
57. Thorsson, V. et al. The immune landscape of cancer. *Immunity* **48**, 812–830 (2018).
58. Saltz, J. et al. Spatial organization and molecular correlation of tumor-infiltrating lymphocytes using deep learning on pathology images. *Cell Rep.* **23**, 181–193 (2018).
59. Virtanen, P. et al. SciPy 1.0: fundamental algorithms for scientific computing in Python. *Nat. Methods* **17**, 261–272 (2020).
60. Hunter, J. D. Matplotlib: a 2D graphics environment. *Comput. Sci. Eng.* **9**, 90–95 (2007). (2007).
61. Waskom, M. L. seaborn: statistical data visualization. *J. Open Source Softw.* **6**, 3021 (2021).
62. Jiang, P. et al. Signatures of T cell dysfunction and exclusion predict cancer immunotherapy response. *Nat. Med.* **24**, 1550–1558 (2018).
63. Butler, A., Hoffman, P., Smibert, P., Papalexi, E. & Satija, R. Integrating single-cell transcriptomic data across different conditions, technologies, and species. *Nat. Biotechnol.* **36**, 411–420 (2018).
64. Wolf, F. A., Angerer, P. & Theis, F. J. SCANPY: large-scale single-cell gene expression data analysis. *Genome Biol.* **19**, 15 (2018).
65. Levine, J. H. et al. Data-driven phenotypic dissection of AML reveals progenitor-like cells that correlate with prognosis. *Cell* **162**, 184–197 (2015).
66. Efremova, M., Vento-Tormo, M., Teichmann, S. A. & Vento-Tormo, R. CellPhoneDB: inferring cell-cell communication from combined expression of multi-subunit ligand-receptor complexes. *Nat. Protoc.* **15**, 1484–1506 (2020).
67. Griffiths, J. A., Richard, A. C., Bach, K., Lun, A. T. L. & Marioni, J. C. Detection and removal of barcode swapping in single-cell RNA-seq data. *Nat. Commun.* **9**, 2667 (2018).
68. McCarthy, D. J., Campbell, K. R., Lun, A. T. & Wills, Q. F. Scater: pre-processing, quality control, normalization and visualization of single-cell RNA-seq data in R. *Bioinformatics* **33**, 1179–1186 (2017).
69. Lun, A. T., McCarthy, D. J. & Marioni, J. C. A step-by-step workflow for low-level analysis of single-cell RNA-seq data with Bioconductor. *F1000Res.* **5**, 2122 (2016).
70. (2023) (2023) (2022) GSEApy: a comprehensive package for performing gene set enrichment analysis in Python Abstract Bioinformatics 39(1) 10.1093/bioinformatics/btac757.
71. Subramanian, A. et al. Gene set enrichment analysis: a knowledge-based approach for interpreting genome-wide expression profiles. *Proc. Natl Acad. Sci. USA* **102**, 15545–15550 (2005).
72. Poon, C. C. et al. Differential microglia and macrophage profiles in human IDH-mutant and -wild type glioblastoma. *Oncotarget* **10**, 3129–3143 (2019).
73. Ochocka, N. et al. Single-cell RNA sequencing reveals functional heterogeneity of glioma-associated brain macrophages. *Nat. Commun.* **12**, 1151 (2021).
74. Zhang, Q. et al. Landscape and dynamics of single immune cells in hepatocellular carcinoma. *Cell* **179**, 829–845 (2019).

Acknowledgements We thank I. Grisse for editorial assistance; P. Gomez for large-scale production of different mouse strains; P. Coulie for comments; and M.-P. Le and M. Formenti for technical assistance. J.Z. was supported by Fondation Contre le Cancer (grant no. 2019-094). This work was supported by WELBIO (Walloon Excellence in Life Sciences and Biotechnology), Belgium (grant no. WELBIO-CR-2019C-05); Fonds pour la Recherche Scientifique (FNRS), Belgium (grant nos EOS O000518F and PDR T.0091.18); Fondation contre le Cancer, Belgium (grant no. 2018-090); Ludwig Cancer Research; and de Duve Institute. The results shown here are in whole or part based on data generated by the TCGA Research Network (https://www.cancer.gov/tcga).

Author contributions J.Z. conceived the project and analysed the data. J.Z. and L.B. performed all of the in vivo experiments. L.B. performed the in vitro experiments. S.N. analysed the single-cell sequencing and bulk RNA-seq data for the MC38-OVA tumour model; L.G. and M.M. analysed the single-cell sequencing data for the TC-1 tumour model. B.J.V.d.E. helped to conceive and design experiments, analyse data and interpret results. J.Z. and B.J.V.d.E. wrote the manuscript. All of the authors were involved in the data interpretation and manuscript preparation.

Competing interests J.Z. and B.J.V.d.E. are listed as inventors on patent applications (WO 2020/083982, WO 2021/214129, Université Catholique de Louvain) related to using α2-AR agonists in cancer immunotherapy. The other authors declare no competing interests.

Additional information

Supplementary information The online version contains supplementary material available at https://doi.org/10.1038/s41586-023-06110-8.

Correspondence and requests for materials should be addressed to Jingjing Zhu.

Peer review information *Nature* thanks Roberta Zappasodi and the other, anonymous, reviewer(s) for their contribution to the peer review of this work. Peer reviewer reports are available.

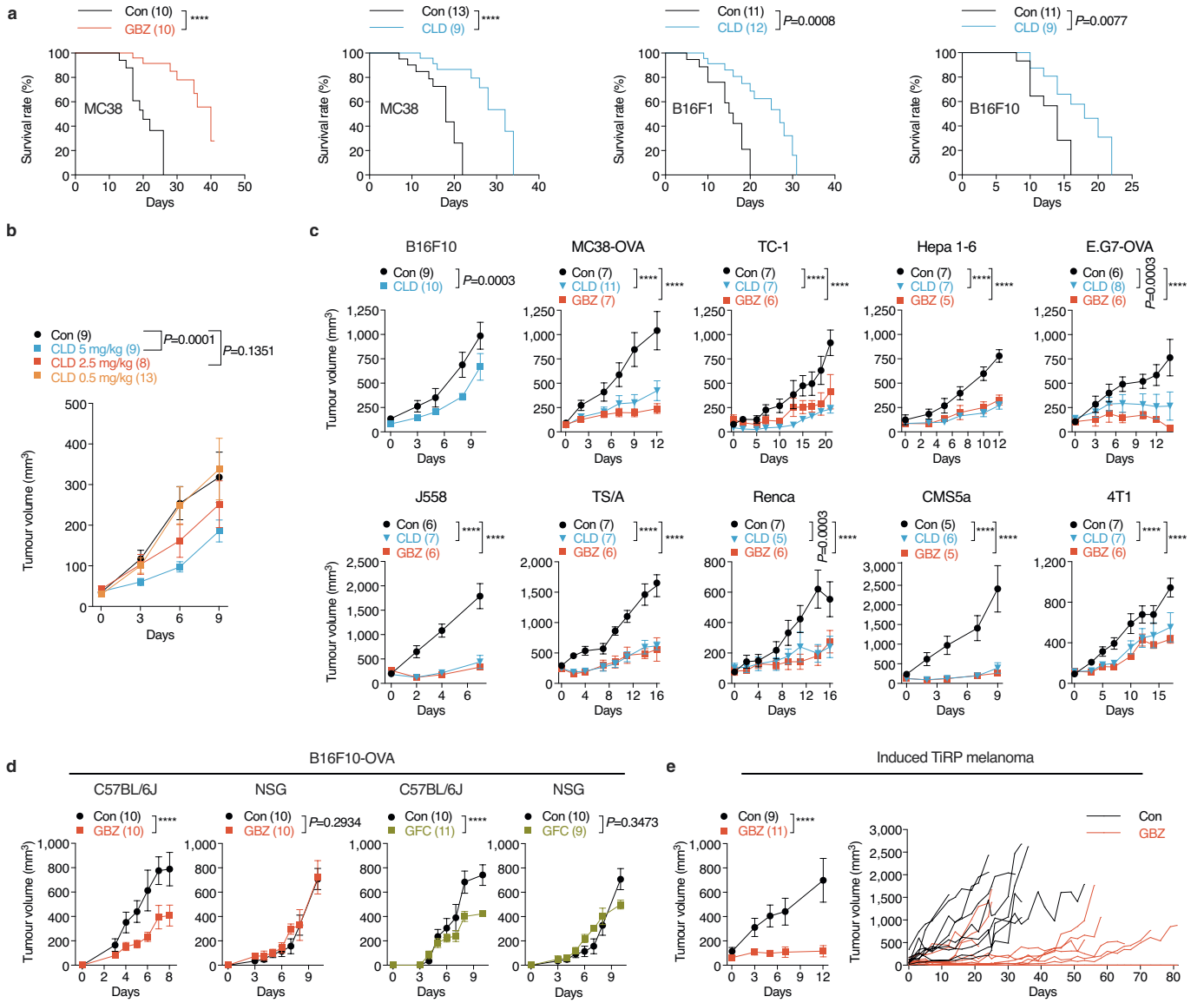

Extended Data Fig. 1 | Anti-tumour effects of clonidine and guanabenz in multiple tumour models. a, Survival curves of mice bearing MC38 colon carcinomas, B16F1 or B16F10 melanomas treated with CLD, GBZ, or vehicle. **b**, Progression of colon carcinomas MC38-OVA in mice treated with different doses of CLD. **c**, Anti-tumour effects of α2-AR agonists as monotherapy in multiple tumour models. GBZ or CLD was given daily (a, c: 5 mg/kg i.p.) starting at day 0 when tumours reached the indicated size. **d**, Progression of melanomas B16F10-OVA in C57BL/6J (immunocompetent) or NSG mice (immunodeficient) treated with vehicle (Con), GBZ or GFC. Data from one representative experiment out of two performed. GBZ (5 mg/kg) or GFC (2 mg/kg) was given daily (i.p.) starting 7 days after tumour implantation (day 0 = start of treatment). **e**, Progression of induced TiRP melanomas in mice treated with vehicle or GBZ. Left: mean growth curve; Right: individual growth curves. GBZ (5 mg/kg) was given daily (i.p.) starting at day 0 when tumours reached around 100 mm^3. The number of mice per group is indicated in brackets. Data (mean ± s.e.m) from one representative experiment out of three (e). P values determined by: ordinary two-way ANOVA (b-e), Log-rank (Mantel-Cox) test was used for the statistical evaluation of survival (a), $p < 0.0001$.

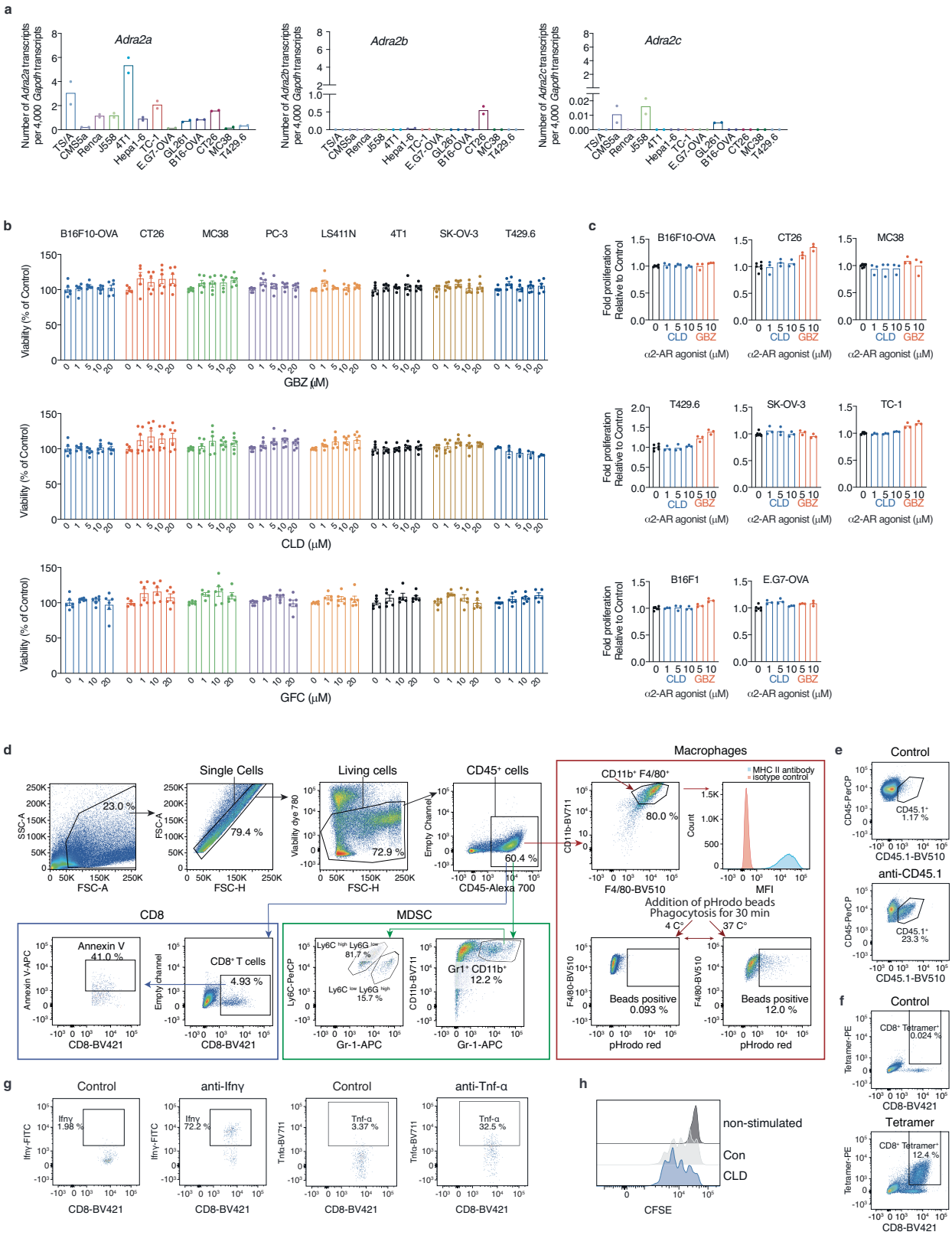

Extended Data Fig. 2 | See next page for caption.

Extended Data Fig. 2 | *Adra2a*, *Adra2b* and *Adra2c* expression in murine tumour cell lines (a), effect of agonists on tumour cell lines *in vitro* (b,c), and gating strategy for flow cytometry analysis of TME cells (d). **a**, Expression of *Adra2a*, *Adra2b* and *Adra2c* in murine tumour cell lines was measured by RT-qPCR. **b**, Effect of α2-AR agonists on cell viability of different tumour cell lines. Cells were treated with different concentrations of GBZ, CLD or GFC for 48 h and cell viability was measured by MTT assay. **c**, Effect of α2-AR agonists on cell proliferation of different tumour cell lines. CFSE assay was used to measure proliferation. During each round of cell division, intracellular CFSE becomes diluted and is quantified (Median fluorescence intensity (MFI) of CFSE) to determine proliferation rate. **d**, Gating strategy on tumour samples for tumour-infiltrating $CD8^+$ T cells (Figs. 1b,d, 2b, 3e,g, 4f,g, Extended Data Figs. 4b,c, 7c), MDSCs (PMN-MDSC: $CD11b^+$ $Gr\text{-}1^{high}$, $Ly6C^{low}$, $Ly6G^{high}$, M-MDSC: $CD11b^+$ $Gr\text{-}1^{low}$, $Ly6C^{high}$, $Ly6G^{low}$) (Fig. 3g, Extended Data Figs. 4c,f, 6f) and macrophages ($CD11b^+$, $F4/80^+$) (Fig. 4e, Extended Data Figs. 6b,c,d,e, 8a,c, 10a). **e**, Gating strategy for Extended Data Fig. 6g. **f**, Gating strategy for Fig. 3g. **g**, Gating strategy for Fig. 3d, Extended Data Fig. 6j. **h**, Gating strategy for Extended Data Fig. 6i. Data (mean ± s.e.m, technical duplicates for a and c, technical sextuplicate for b) from one representative out of two independent experiments.

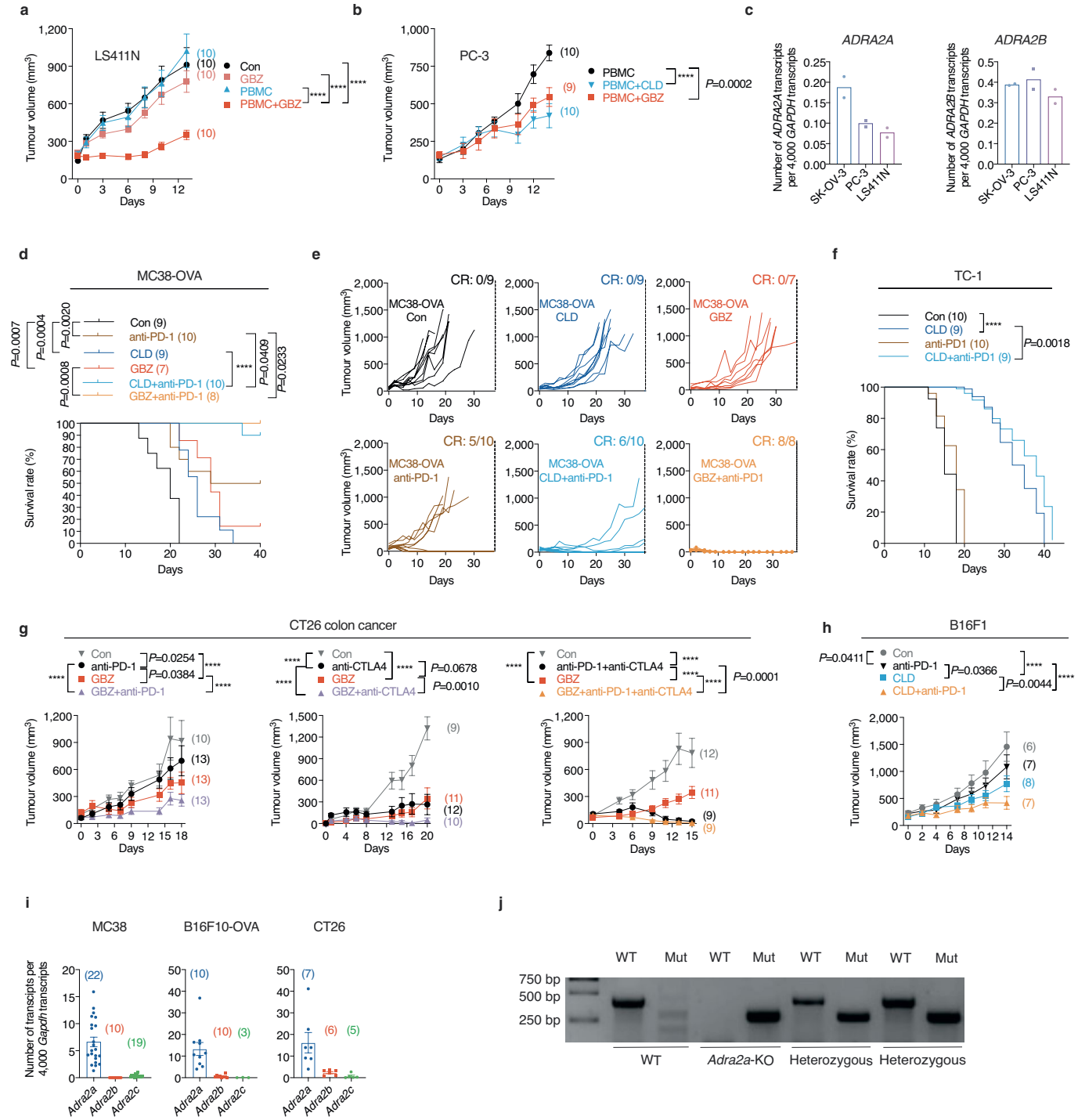

Extended Data Fig. 3 | See next page for caption.

Extended Data Fig. 3 | Effect of α2-AR agonists on human tumour xenografts in humanized models (a-c), combination of α2-AR agonists with ICB (d-h), and genotyping of *Adra2a*-KO mice (ij). a-b, Progression of human xenografts of colorectal carcinomas LS411N (a) or prostate carcinomas PC-3 (b) in NSG mice (immunodeficient) treated with vehicle, GBZ or CLD after adoptive transfer of allogeneic human PBMC. Human PBMC were injected (i.v.) on day 0 when tumours reached the indicated size. Treatments (5 mg/kg daily i.p.) started on the same day. Mean ± s.e.m from one representative out of two independent experiments. **c**, Expression of *ADRA2A* and *ADRA2B* in human tumour cell lines measured by RT-qPCR. Data from one representative out of two independent experiments. **d**, Survival of MC38-OVA tumour-bearing mice treated with GBZ, CLD and/or anti-PD-1, as indicated. **e**, Individual tumour growth curves for mice from (d) (CR: complete tumour rejection). **f**, Survival of TC-1 tumour-bearing mice treated with CLD, anti-PD-1 or both. **g**, Progression of colon carcinomas CT26 in mice treated with GBZ, anti-PD-1, anti-CTLA4, or combinations of these. Treatments started on day 0 (7 days after tumour implantation). **h**, Progression of melanomas B16F1 in mice treated with CLD, anti-PD-1, or both. CLD and GBZ were given daily (5 mg/kg i.p.) starting at day 0 when tumours reached the indicated size. Anti-CTLA4 (40 μg) and anti-PD-1 (200 μg) antibodies (i.p.) were given 1 day before the first injection of α2-AR agonists, then twice a week. **i**, Expression of *Adra2a*, *Adra2b* and *Adra2c* measured by RT-qPCR in bulk tissue from MC38, B16F10-OVA and CT26 tumours. Each dot represents an individual mouse. **j**, Genotyping of *Adra2a*-KO mice. Genotyping was performed by PCR on genomic DNA from mouse tails, using primers described in the materials and methods. Mice with only the mutant band detected are identified as *Adra2a*-KO mice. Shown is the genotyping result for one batch of mice. Genotyping was repeated for all mice used. For gel source data, see Supplementary Fig. 1a. Mean ± s.e.m. P values determined by: ordinary two-way ANOVA (a,b,g,h), Log-rank (Mantel-Cox) test was used for the statistical evaluation of mouse survival (d and f), **** $p < 0.0001$.

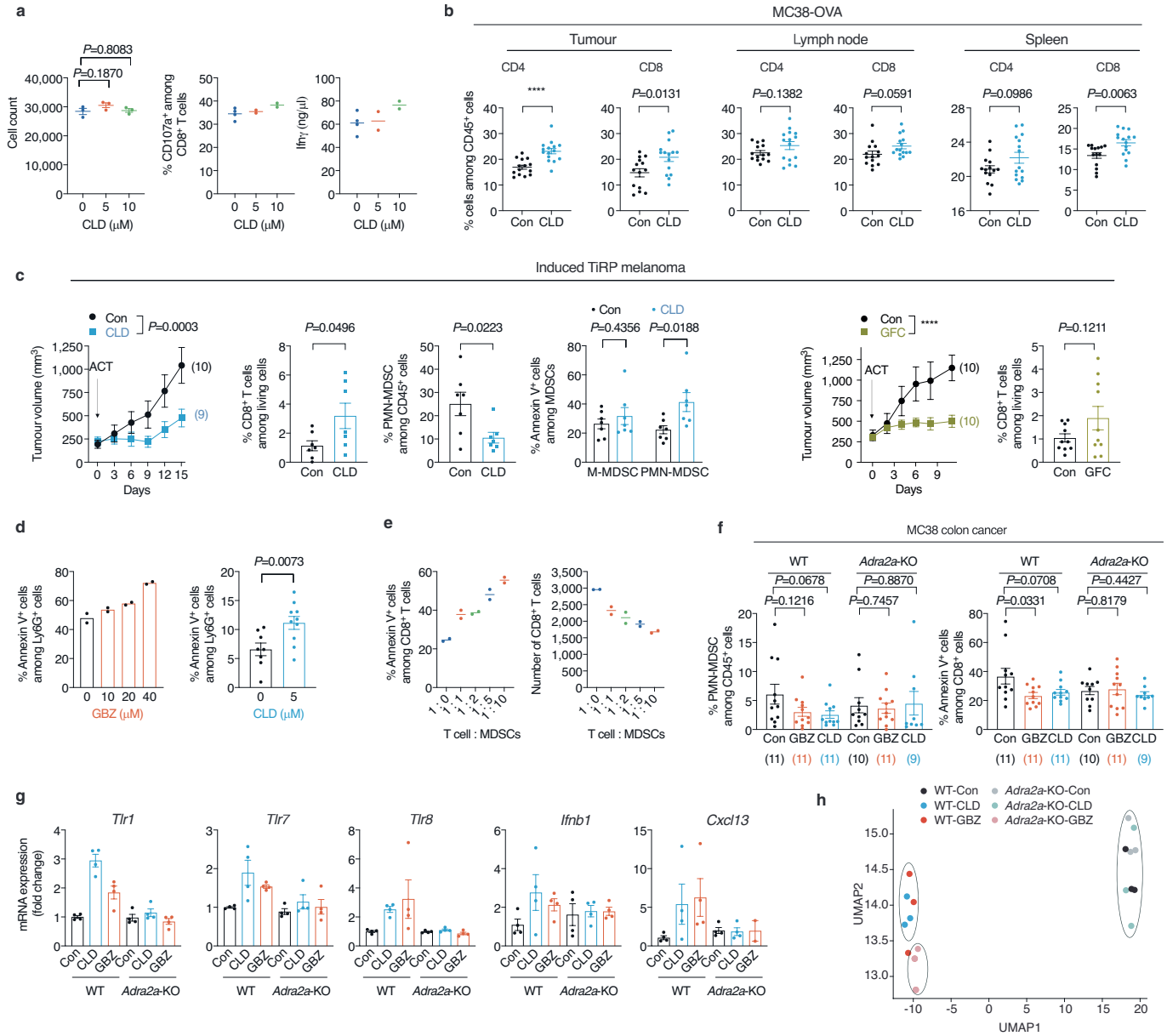

Extended Data Fig. 4 | Effect of clonidine on T cells and myeloid cells (a-f), and transciptomic analysis of treated tumours (g-h). **a**, Effect of CLD on TCRP1A CD8$^+$ T-cell proliferation *in vitro* (left panel) and activity as measured by T-cell degranulation (middle panel) and Ifn-γ ELISA (right panel). **b**, CD4$^+$ and CD8$^+$ T-cell infiltration in tumours, lymph nodes and spleens of MC38-OVA tumour-bearing mice analysed by flow cytometry after 7 days of treatment with vehicle (n = 14) or CLD (n = 15). CLD was given daily by i.p. injections (5 mg/kg) starting when tumours reached 50 mm^3, and T-cell analysis was performed 7 days later. **c**, Progression, CD8$^+$ T-cell infiltration and PMN-MDSC infiltration/apoptosis, of induced TiRP melanomas in TiRP mice treated with CLD or GFC after ACT of 10 million activated TCRP1A CD8$^+$ T cells. **d**, GBZ and CLD induce apoptosis of PMN-MDSC *in vitro*. PMN-MDSCs were isolated from induced TiRP melanomas using MDSC isolation kit (Miltenyi Biotec) and were cultured and treated with GBZ or CLD for 24 h. Apoptosis was analysed by flow cytometry using Annexin V. **Left:** technical duplicate from one representative experiment out of two independent experiments; **Right:** Data pooled from technical duplicates/triplicates of MDSCs isolated from 4 different batches of mice (mean ± s.e.m.). **e**, T-cell suppressive activity of Ly6G$^+$ myeloid cells (PMN-MDSC) isolated from induced TiRP melanomas, as measured by T-cell apoptosis (left) and T-cell number after co-culture (right). Technical duplicates from one representative experiment out of two. **f**, PMN-MDSC infiltration and CD8$^+$ T-cell apoptosis in MC38 tumours from wild-type or *Adra2a*-KO mice treated with vehicle, GBZ or CLD. CLD, GBZ (5 mg/kg) and GFC (2 mg/kg) were given daily (i.p.), starting on day 0 when tumours reached the indicated size. Tumours were analysed *ex vivo* on day 6. **g**, RT-qPCR confirmation of mRNA expression of selected genes identified in the RNA-seq analysis. Mean fold change relative to untreated wild-type mice ± s.e.m. for MC38-OVA tumours from wild-type or *Adra2a*-KO mice treated with CLD and GBZ, as explained in f. Mean ± s.e.m, n = 4 independent biological samples. **h**, UMAP projection of L1-normalised gene expression using the genes of the upregulated (Post_Up) and the downregulated (Post_Down) signatures as defined in Supplementary Table 2, highlighting differences between MC38-OVA tumours from wild-type and *Adra2a*-KO mice treated with CLD or GBZ, as compared to untreated tumours (6 conditions, n = 3 per group). Clusters were identified with hierarchical clustering, using Spearman correlations between the samples as distance measure. Data (mean ± s.e.m) from one representative experiment out of two independent experiments (a–f). P values determined by: ordinary two-way ANOVA (c), *t*-test (Unpaired, two-tailed) (columns, a,b,c,d,f), **** $p < 0.0001$.

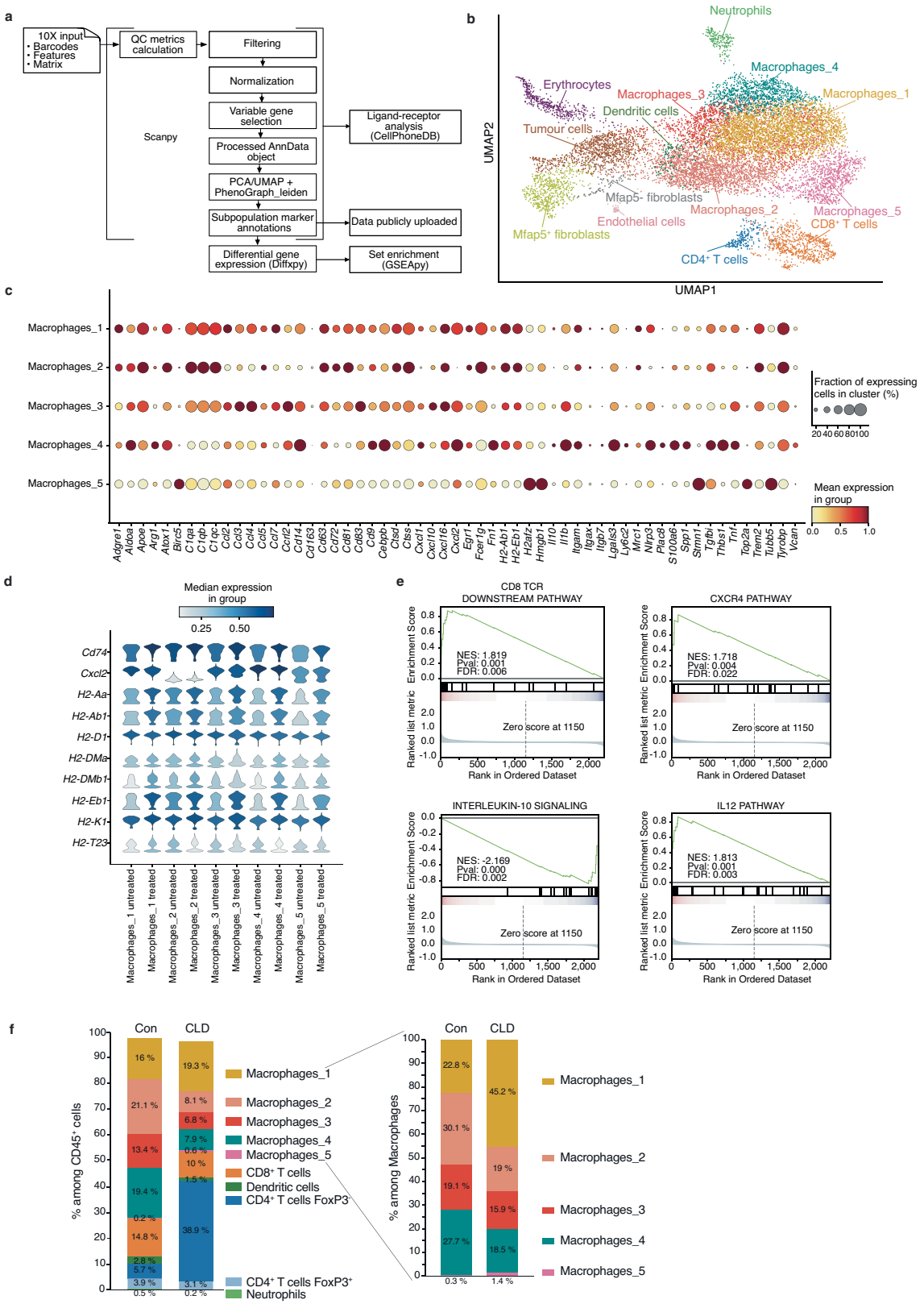

Extended Data Fig. 5 | See next page for caption.

Extended Data Fig. 5 | Single-cell RNAseq analysis of tumours from mice treated or not with clonidine (CLD). a, Schematic representation of the scRNAseq workflow. **b**, UMAP representation of the merged dataset for treated and untreated MC38-OVA tumours. See Supplementary Table 1 for the markers used for cluster identification. **c**, Dotplot representing highly variable genes with relevance for macrophage activation. See main text for a description of the markers defining clusters 1 and 3. Cluster 2 is characterized by high expression of *Fcer1g, Tyrobp, Cd7, C1qa, C1qb, Cd72, Trem2*, and is similar to the anti-inflammatory macrophages as described before[72]. Cluster 4 is characterized by high expression of *Thbs1, Lgals3, Fn1, Arg1, Ly6c2* and *Tgfbi* and is hence similar to the described population of intermediate monocyte-macrophage[73]. In another paper, these cells were identified as MDSC-like macrophages[74]. Cluster 5 is characterized by a high expression of genes encoding proliferation-related proteins (*Tubb5, Stmn1, Hmgb1, H2afz and Top2a*). **d**, Violin plots (Scanpy) showing the effect of CLD treatment on expression of 10 differentially expressed genes associated with H2 (two-sided Wilcoxon rank sum test with Benjamini-Hochberg correction for multiple testing, p.adj < 10-5) in each of the macrophage subpopulations versus the dataset mean. **e**, Enrichment plots (GSEA) in $CD8^+$ T cells indicate an increase in $CD8^+$ T-cell activation, which coincides with an increased $CD8^+$ T cell infiltration shown in Fig. 4b. **f**, Single cell RNAseq analysis of TC-1 lung carcinomas treated or not with CLD. Relative proportions of immune cells in each cluster based on the unsupervised shared nearest-neighbour graph clustering of TC-1 tumours (pools of 10 tumours per group). Class identities were assigned using reference-based cell type annotations using the MC38-OVA tumours (see Fig. 4) as reference. The apparent reduction of macrophages in treated samples is only relative, and results from the increased proportion of $CD4^+$ T cells.

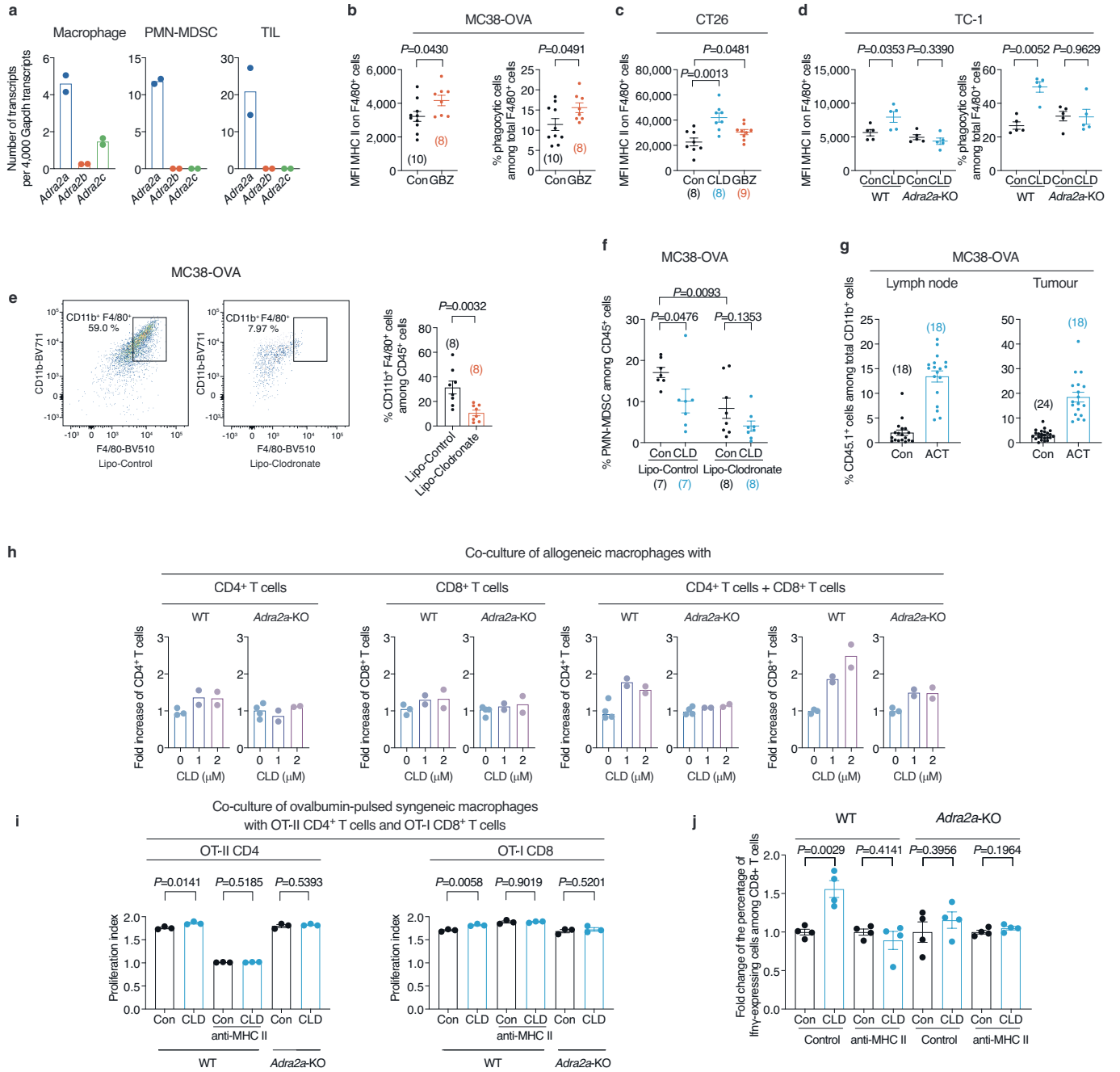

Extended Data Fig. 6 | Role of macrophages in the anti-tumour effect of α2-AR agonists. a, Expression of *Adra2a, Adra2b* and *Adra2c* in macrophages (CD11b$^+$, F4/80$^+$, MHC II$^+$), PMN-MDSCs (CD11b$^+$, Gr1$^+$ Ly6G^{high} Ly6C^{low}) and CD8$^+$ T cells (CD45$^+$ CD8$^+$) sorted from MC38-OVA tumours (a pool of 8 tumours) by BD FACSAria™ III Cell Sorter. Technical duplicates from one representative experiment out of two. **b**, Surface MHC II expression and phagocytic activity of TME macrophages from MC38-OVA tumours in mice treated with vehicle or GBZ. **c**, Surface MHC II expression of TME macrophages from CT26 tumours in mice treated with vehicle, CLD or GBZ. **d**, Surface MHC II expression (left) and phagocytic activity (right) of TME macrophages from TC-1 tumours in wild-type or *Adra2a-KO* mice treated with vehicle or CLD (n = 5 per group). **e**, Efficiency of macrophage depletion by liposomal clodronate. Representative flow cytometry dot plots (left) and statistic bar graph (right) showing the efficacy of macrophage depletion following *in vivo* administration of liposomal clodronate to MC38-OVA tumour-bearing mice, as indicated in Fig. 4f. **f**, Depletion of PMN-MDSCs by liposomal clodronate. The abundance of PMN-MDSCs in tumours was evaluated by flow cytometry following CLD treatment and *in vivo* administration of liposomal clodronate to MC38-OVA tumour-bearing mice. Mean ± s.e.m. n = 7, 7, 8, 8 biologically independent samples. **g**, Migration of adoptively transferred CD45.1$^+$ macrophages into lymph nodes and tumours of MC38-OVA tumour-bearing mice (CD45.2). Drugs were administered daily by i.p. injection: GBZ, CLD, 5 mg/kg. Treatments started when tumours reach around 100 mm^3. Mice were euthanized after 4 days of treatment. **h**, Effect of CLD on the proliferation of murine allogeneic CD4$^+$ and CD8$^+$ T cells co-cultured with WT or *Adra2a*-KO macrophages. T cells were counted by flow cytometry. Technical duplicates from one representative experiment out of three . **i**, Effect of CLD (2.5 μM) on the proliferation of murine OT-II CD4$^+$ and OT-I CD8$^+$ T cells estimated by CFSE dilution after co-culture with WT or *Adra2a*-KO syngeneic macrophages pulsed with ovalbumin protein. An anti-MHC II monoclonal antibody (50 μg ml^{-1}) was added as indicated. Technical triplicates from one representative experiment out of three. **j**, Ifn-γ production by OT-I CD8$^+$ T cells co-cultured as in (i) and stimulated with E.G7-OVA tumour cells for 16 h. Intracellular Ifn-γ was measured by flow cytometry. Each dot represents the mean of technical duplicates. n = 4 independent biological replicates. Data (mean ± s.e.m) from one representative experiment out of three (b–f,i) except for g (all mice shown). P values determined by t-test (Unpaired, two-tailed) (b,d,f,i,j). **** p < 0.0001.

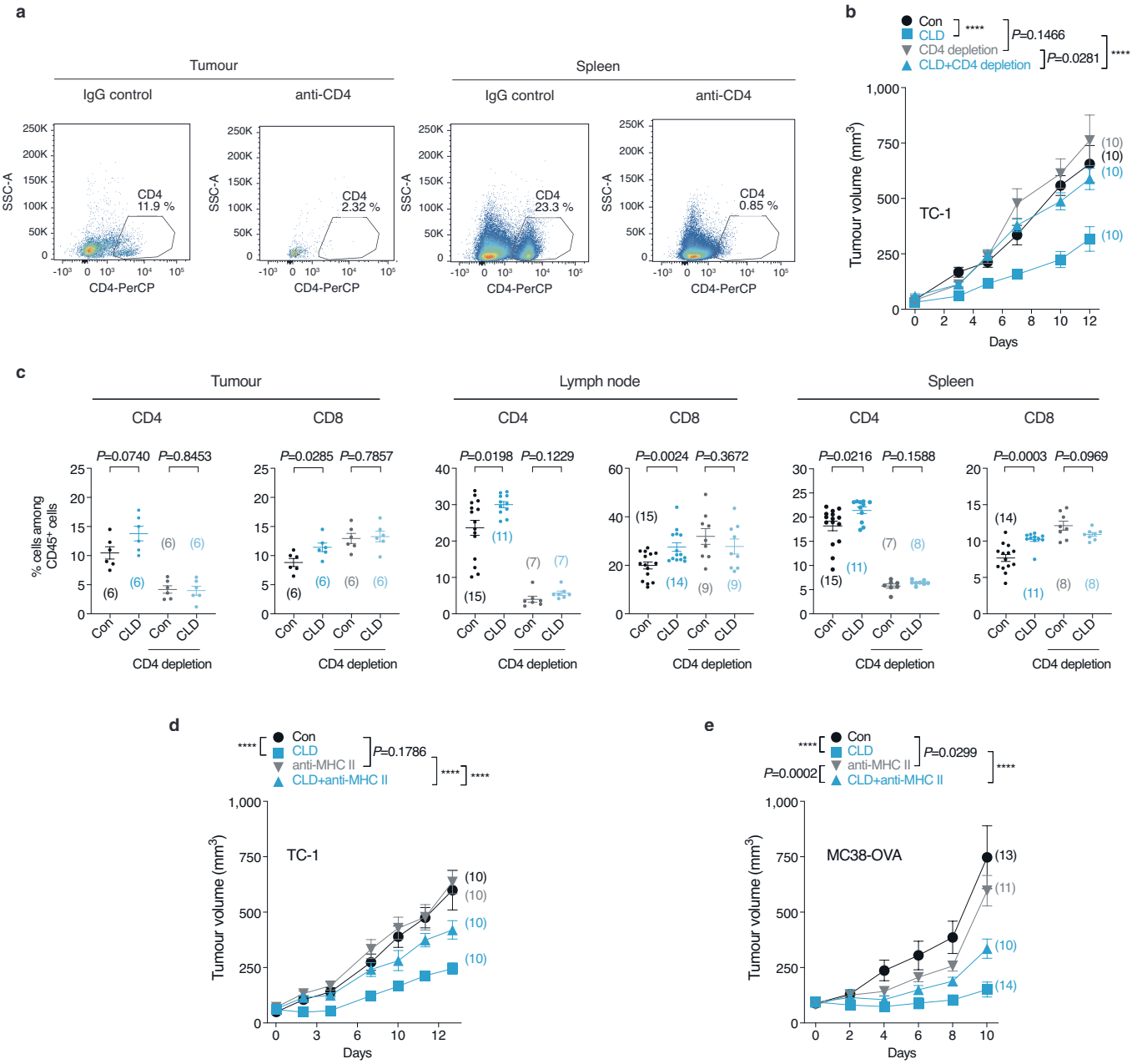

Extended Data Fig. 7 | Role of CD4$^+$ T cells in the effects of α2-AR agonists. **a**, Representative flow cytometry dot plots showing the efficacy of CD4$^+$ T-cell depletion following *in vivo* administration of the anti-CD4 mAb in tumour (left) and spleen (right). **b**, Progression of TC-1 tumours in mice treated with CLD, anti-CD4, or both. **c**, Infiltration of CD4$^+$ and CD8$^+$ T cells in the tumour, lymph node and spleen of TC-1 tumour-bearing mice treated with CLD, anti-CD4, or both. The apparently increased CD8$^+$ T cell proportion in CD4-depleted samples is only relative, and so appears because of the disappearance of CD4$^+$ T cells in those samples. **d** and **e**, Progression of TC-1 (d) or MC38-OVA (e) tumours in mice treated with CLD, anti-MHC II, or both. CLD was given daily (5 mg/kg i.p.) starting at day 0 when tumours reached the indicated size. Anti-CD4 antibody (500 µg) was given 1 day before starting CLD treatment, then 250 µg twice per week. Anti-MHC II (500 µg) antibody (i.p.) was given 1 day before the first injection of CLD, then twice a week. Data (mean ± s.e.m) from one representative out of three independent experiments (c) except for b,d and e (all mice shown). P values determined by: ordinary two-way ANOVA (b,d,e), t-test (Unpaired, two-tailed) (c). **** $p < 0.0001$.

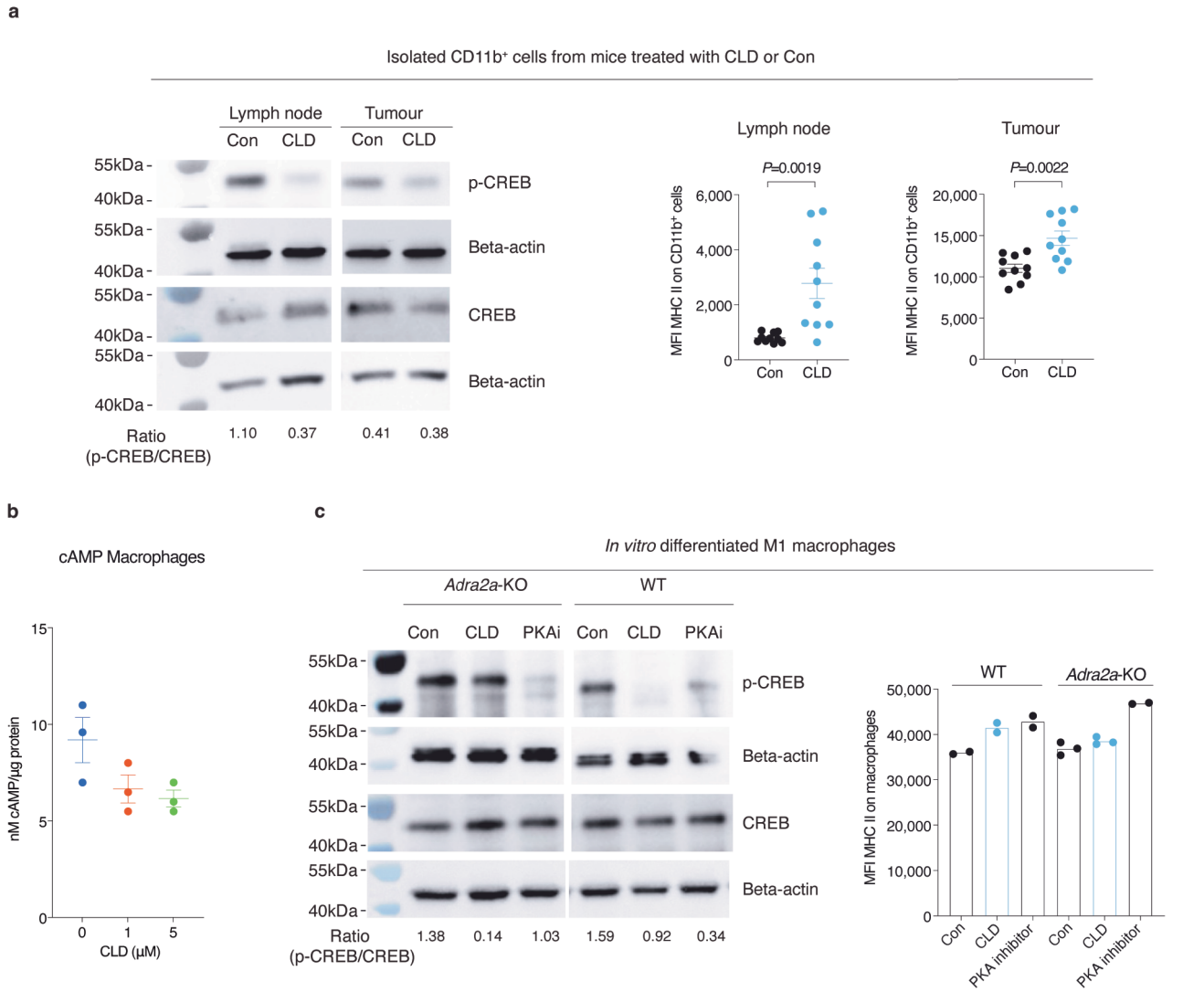

Extended Data Fig. 8 | Effects of α2-AR agonists on the cAMP-PKA signalling pathway. a, MC38-tumour bearing mice (10 mice per group) were treated with CLD or vehicle for 7 days. Tumours and lymph nodes were collected and pooled for isolation of CD11b$^+$ cells. Left panels: Cell lysates were analysed for phospho-CREB and total CREB by western blotting. Beta-actin was used as loading control. The phospho-CREB to total CREB ratio is indicated below the blots. Right panels: MHC II expression of CD11b$^+$ cells in the lymph nodes and tumours from the same mice used in the left panels. **b**, Quantification of cAMP levels in *in vitro* differentiated M1 macrophages treated with different concentrations of CLD for 15 min. Mean ± s.e.m of one experiment (technical triplicates). **c**, M1 macrophages differentiated *in vitro* from WT or *Adra2a*-KO bone marrow cells were treated with CLD (2.5 µM) for 16 h. Cell lysates were then analysed for phospho-CREB and total CREB by western blotting (left panels). Macrophages treated with PKA inhibitor (H-89 dihydrochloride hydrate, 1 µM) were used as controls. Beta-actin was used as loading control. The phospho-CREB to total CREB ratio is indicated below the blots. MHC II expression by the same cells is shown on the right panel. For gel source data, see Supplementary Fig. 1b and c. Data (mean ± s.e.m) from one representative out of two independent experiments (a,c). P values determined by *t*-test (Unpaired, two-tailed). **** $p < 0.0001$.

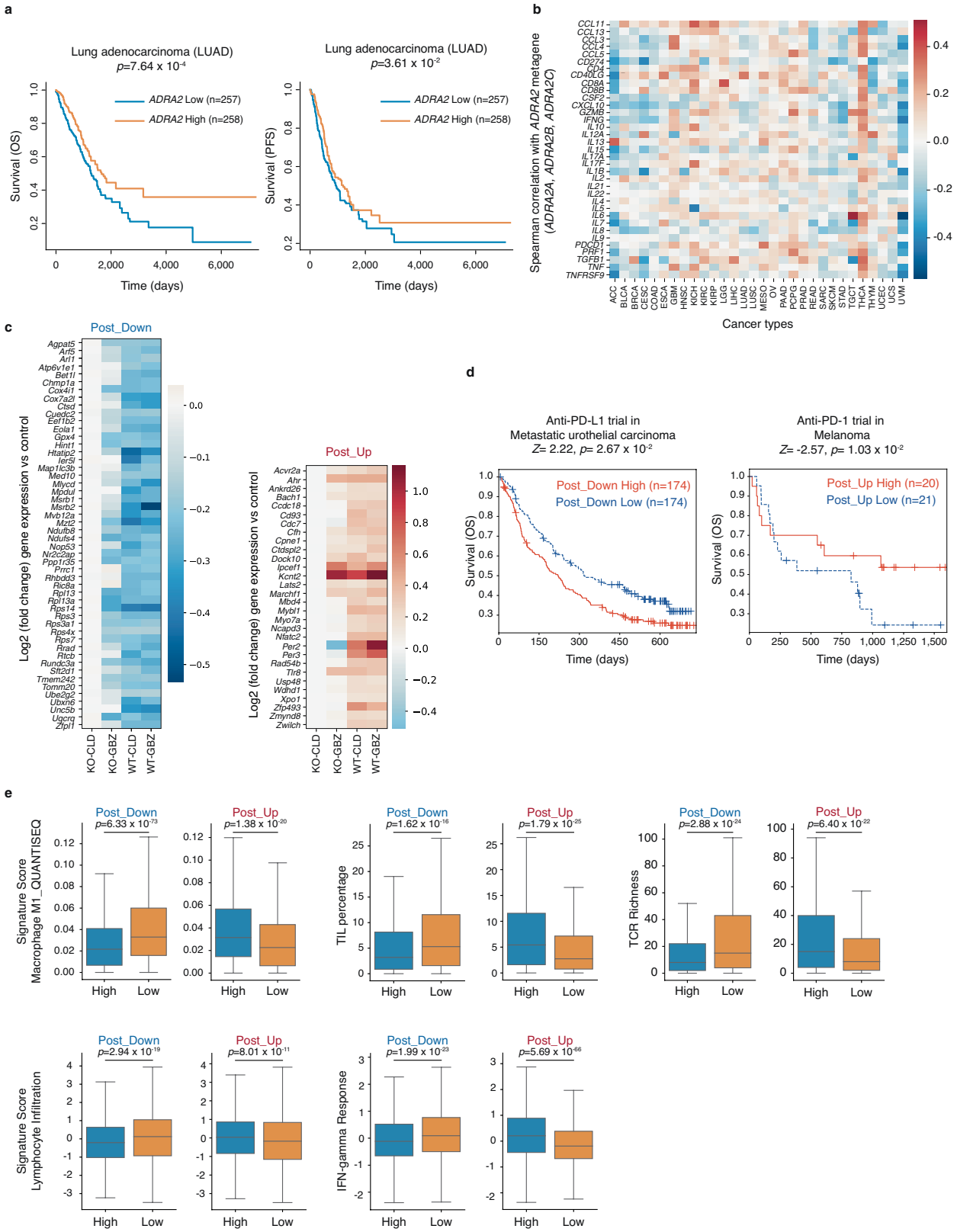

Extended Data Fig. 9 | See next page for caption.

Extended Data Fig. 9 | Association of α2-AR tumour signalling with survival of patients with cancer. a, Kaplan–Meier curves for Overall Survival (OS) and Progression-free Survival (PFS) related to *ADRA2* metagene (sum of *ADRA2A, ADRA2B, ADRA2C*) expression in human lung adenocarcinoma (LUAD) analysed using clinical data from TCGA (n = 515). **b**, Heatmap showing correlation of the expression of immune modulators genes with *ADRA2* metagene expression across the TCGA cancer types (30 cancer types; ACC: n = 77, BLCA: n = 413, BRCA: n = 1130, CESC: n = 304, COAD: n = 331, ESCA: n = 181, GBM: n = 158, HNSC: n = 518, KICH: n = 66, KIRC: n = 542, KIRP: n = 288, LGG: n = 508, LIHC: n = 369, LUAD: n = 537, LUSC: n = 503, MESO: n = 87, OV: n = 423, PAAD: n = 178, PCPG: n = 176, PRAD: n = 503, READ: n = 91, SARC: n = 258, SKCM: n = 102, STAD: n = 414, TGCT: n = 132, THCA: n = 504, THYM: n = 119, UCEC: n = 189, UCS: n = 57, UVM: n = 79). **c**, Heatmaps showing the expression fold changes of genes downregulated (Post_Down) or upregulated (Post_Up) by CLD and GBZ in MC38-OVA tumours from WT or *Adra2a*-KO mice, as compared to untreated tumours (6 conditions, n = 3 per group). **d**, Cox Proportional Hazards (CoxPH) regression analysis across clinical trials in TIDE[37,38] (BLCA: n = 348, SKCM: n = 41), using as input the human ortholog genes of the up- and downregulated gene signatures post treatment with CLD or GBZ (Post_Up and Post_Down). Negative Z-scores indicate better survival in the high expression group per signature. **e**, Boxplots highlighting statistically significant differences between high and low expression of the Post_Up and Post_Down gene signatures across a set of immune parameters calculated for TCGA (n = 9320, 30 cancer types). Groups were selected based on median expression of Post_Up or Post_Down signatures. Boxes represent the median, 1st and 3rd quartiles; outliers were determined based on the interquartile range and ignored for visualization. P values are determined by Log-rank-test (a), CoxPh regression-test (d), Two-sidedWelch *t*-tests (e). $p < 0.05$ is considered significant.

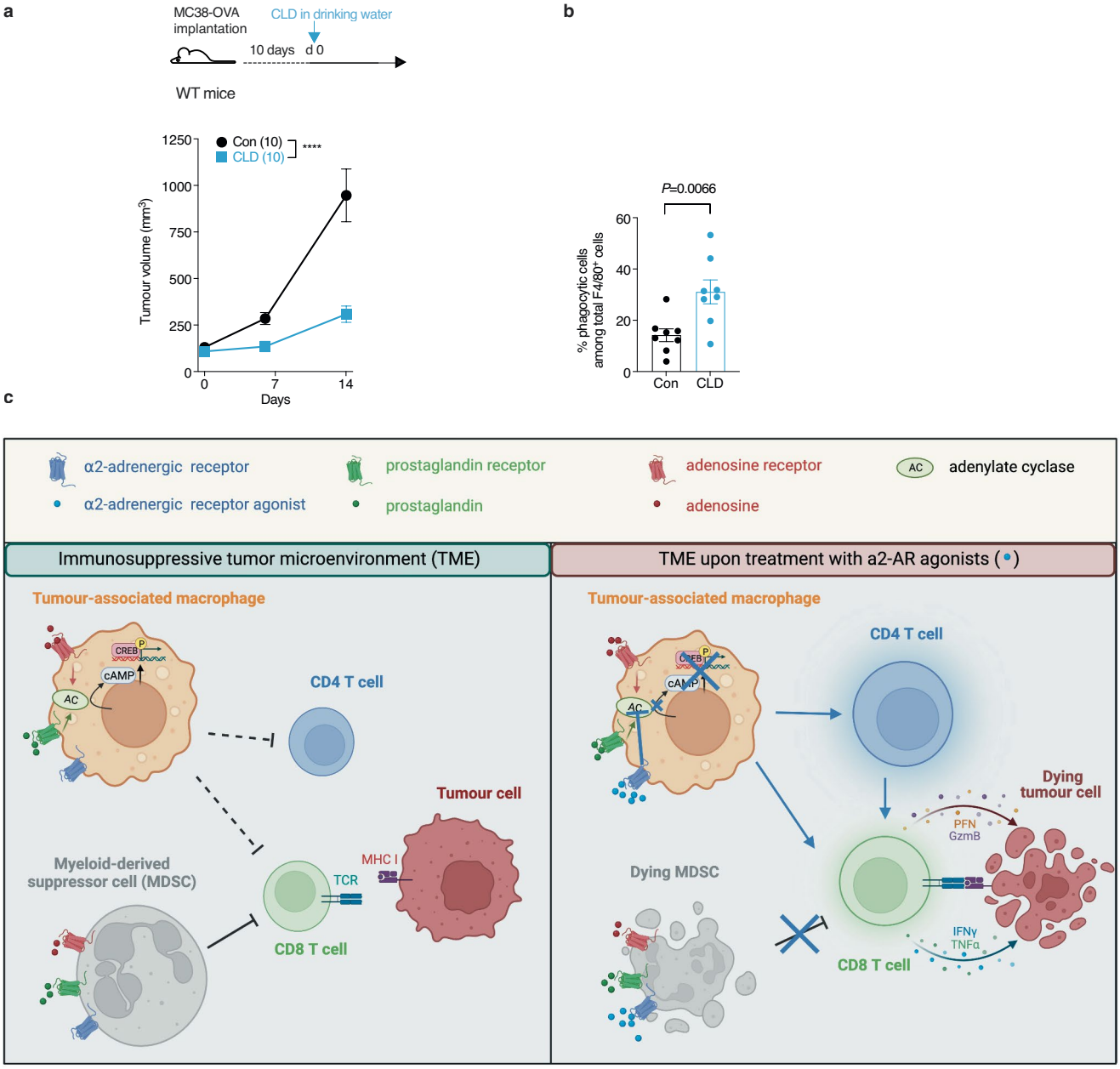

Extended Data Fig. 10 | Anti-tumour effect of clonidine administered via the oral route (a,b), and schematic model of the anti-tumour activity of α2-AR agonists (c). a, Progression of MC38-OVA colon carcinomas in mice treated with drinking water supplemented with clonidine (CLD) (10 μg ml^{-1}). **b**, Phagocytic activity of TME macrophages from mice treated in (a) (n = 8 per group). Data (mean ± s.e.m) from one representative out of three independent experiments. P values determined by ordinary two-way ANOVA (left) and *t*-test (Unpaired, two-tailed, right). **** p < 0.0001. **c**, Model of the identified mechanisms underlying the anti-tumour activity of α2-AR agonists in the context of immunotherapy. Tumour-associated macrophages and myeloid-derived suppressor cells (MDSCs) contribute to immunosuppression in the tumour microenvironment, partly in response to factors such as adenosine and prostaglandins, which trigger the cAMP/pCREB signalling pathway. Agonists of the α2-adrenergic receptor (blue) inhibit adenylate cyclase (AC), thereby blocking the immunosuppressive cAMP/pCREB signalling. Macrophages now better stimulate anti-tumour CD4 and CD8 T cells, while MDSCs die by apoptosis. The schematic in **c** was created using BioRender.

nature research

Corresponding author(s): Jingjing Zhu

Last updated by author(s): March 28

Reporting Summary

Nature Research wishes to improve the reproducibility of the work that we publish. This form provides structure for consistency and transparency in reporting. For further information on Nature Research policies, see our Editorial Policies and the Editorial Policy Checklist.

Statistics

For all statistical analyses, confirm that the following items are present in the figure legend, table legend, main text, or Methods section.

n/a	Confirmed	
☐	☒	The exact sample size (*n*) for each experimental group/condition, given as a discrete number and unit of measurement
☐	☒	A statement on whether measurements were taken from distinct samples or whether the same sample was measured repeatedly
☐	☒	The statistical test(s) used AND whether they are one- or two-sided *Only common tests should be described solely by name; describe more complex techniques in the Methods section.*
☐	☒	A description of all covariates tested
☐	☒	A description of any assumptions or corrections, such as tests of normality and adjustment for multiple comparisons
☐	☒	A full description of the statistical parameters including central tendency (e.g. means) or other basic estimates (e.g. regression coefficient) AND variation (e.g. standard deviation) or associated estimates of uncertainty (e.g. confidence intervals)
☐	☒	For null hypothesis testing, the test statistic (e.g. *F*, *t*, *r*) with confidence intervals, effect sizes, degrees of freedom and *P* value noted *Give P values as exact values whenever suitable.*
☒	☐	For Bayesian analysis, information on the choice of priors and Markov chain Monte Carlo settings
☒	☐	For hierarchical and complex designs, identification of the appropriate level for tests and full reporting of outcomes
☐	☒	Estimates of effect sizes (e.g. Cohen's *d*, Pearson's *r*), indicating how they were calculated

Our web collection on statistics for biologists contains articles on many of the points above.

Software and code

Policy information about availability of computer code

Data collection

- scRNAseq and RNAseq were obtained from in-house experiments. See Data section.
- Data from public sources were either obtained from TIDE for the clinical trials (http://tide.dfci.harvard.edu/login/), or the Toil-recompute initiative part of Xena for the TCGA data (https://xenabrowser.net/datapages/?host=https%3A%2F%2Ftoil.xenahubs.net&removeHub=https%3A%2F%2Fxena.treehouse.gi.ucsc.edu%3A443).
- Immune deconvolutions were obtained from TIMER (http://timer.cistrome.org).
- Derived TCGA metrics from the Thorsson et al (2018) landscaping project, were downloaded from the GDC portal associated with their manuscript (https://gdc.cancer.gov/about-data/publications/panimmune).
- All data sources have been defined in the corresponding methods sections.
- Code to generate supplementary figures is available on Zenodo under DOI: 10.5281/zenodo. 7789646 (https://doi.org/10.5281/zenodo.7789646).
- Code for Data processing and analysis are available on Github (https://github.com/BVDElab/Tumour_immune_rejection) and archived on Zenodo under DOI: 10.5281/zenodo.7751788 (https://doi.org/10.5281/zenodo.7751788).
- Public data associated with the clinical trial survival analyses can be consulted at http://tide.dfci.harvard.edu/login/. All pre-processed TCGA metrics can be freely accessed at https://gdc.cancer.gov/about-data/publications/panimmune.

Data analysis

-The following software implementations were used for in vitro and in vivo data analysis: Flowjo Flowjo version 10.7.2, GraphPad Prism version 8.4.3 and Microsoft Excel for Mac version 16.7.
- scRNA sequencing data were processed with CellRanger version (6.1.2).
- Python scRNA-seq and RNA-seq analyses: Python (3.7.3), Scanpy (1.7.0), Phenograph (1.5.7), Diffxpy (0.7.4), CellPhoneDB (2.0), SciPy (1.7.1), GSEApy (0.10.5), scikit-learn (0.24.1) and UMAP-learn (0.5.1).
- Python visualisation: Python (3.8.8), matplotlib (3.5.2), seaborn (0.11.1).
- R scRNA-Seq analyses: R (4.2.0 Patched, 2022-05-13 r82357), SingleCellExperiment (1.18.0), DropletUtils (1.16.0), scuttle (1.16.3), scran

(1.24.1), SingleR (1.10.0), scater (1.24.0), AnnotationHub (3.4.0), tidyverse (1.3.2), celldex (1.6.0), bluster (1.6.0). A detailed list with all dependencies and versions is available in the code for data processing and analysis repository (https://github.com/BVDElab/Tumour_immune_rejection). scRNA-Seq analyses with Seurat (4.0.3) were performed with R 4.0.3.
- RNAseq analysis: R (4.0.3), tximport (1.20.0), TxDB (3.10) and DEseq2 (1.32.0). Reads were mapped using Kallisto (0.46.0) and processed with trim_galore (0.6.5).
- Survival analyses were either performed using the TIDE web portal (http://tide.dfci.harvard.edu/login/) or with the package lifelines (0.26.3).

For manuscripts utilizing custom algorithms or software that are central to the research but not yet described in published literature, software must be made available to editors and reviewers. We strongly encourage code deposition in a community repository (e.g. GitHub). See the Nature Research guidelines for submitting code & software for further information.

Data

Policy information about availability of data

All manuscripts must include a data availability statement. This statement should provide the following information, where applicable:

- Accession codes, unique identifiers, or web links for publicly available datasets
- A list of figures that have associated raw data
- A description of any restrictions on data availability

- Raw datasets have been uploaded to GEO under accessions GSE227601 (scRNA-seq) and GSE226290 (bulk RNA-seq).
- Data to generate supplementary figures is available on Zenodo under DOI: 10.5281/zenodo. 7789646 (https://doi.org/10.5281/zenodo.7789646).
- Data to repeat processing analysis are available on Github (https://github.com/BVDElab/Tumour_immune_rejection) and archived on Zenodo under DOI: 10.5281/zenodo.7751788 (https://doi.org/10.5281/zenodo.7751788).
-Public data associated with the clinical trial survival analyses can be consulted at http://tide.dfci.harvard.edu/login/. All pre-processed TCGA metrics can be freely accessed at https://gdc.cancer.gov/about-data/publications/panimmune.
- Mouse reference genome: GRCm38.96
- Ortholog annotation: BioMart release 104.

Field-specific reporting

Please select the one below that is the best fit for your research. If you are not sure, read the appropriate sections before making your selection.

☒ Life sciences ☐ Behavioural & social sciences ☐ Ecological, evolutionary & environmental sciences

For a reference copy of the document with all sections, see nature.com/documents/nr-reporting-summary-flat.pdf

Life sciences study design

All studies must disclose on these points even when the disclosure is negative.

Sample size	No statistical methods were used to determine the sample size. The sample size was chosen based on preliminary experiments and previously published results. The group size for each individual experiment is mentioned on the graph itself or in the figure legend. For Single cell analysis: 2 tumour samples (pool of 10 tumours in each group) from MC38-OVA tumor-bearing mice treated with Clonidine or PBS. 2 tumour samples (pool of 10 tumours in each group) from TC-1 tumour-bearing mice treated with Clonidine or PBS. For the RNAseq data, all treatments were analysed in triplicate. TCGA or public clinical trial data was processed as provided by the public repositories. Sample sizes are references in the corresponding figure and/or legends. Not applicable for computational or systems biology-based re-analyses of existing (publicly available) patient cohorts (TCGA, TIDE), since almost all of the computational analyses exploited already published clinical patient cohorts wherein sample sizes were predetermined by the original study investigators.
Data exclusions	There were no deliberate data exclusions. For Flow cytometry of in vivo experiment: Samples are excluded if the number of events in the targeting population is below 100. In the scRNA-seq analysis, quality control metrics were calculated with Scanpy 1.7.0. Cells with either low (<200) or higher than expected (>2,500) number of individual genes expressed were excluded from the downstream analysis.
Replication	Reproducibility of experimental findings (wherever applicable) was verified by either considering analyses of multiple patient samples, high number of single-cells, and/or equal to at least or more than 3 biologically independent experiments. All attempts at replication were successful. We did not perform replication for the 10X Chromium assay, however, each sample was pooled from multiple mouse tumors, as indicated. RNAseq was performed in triplicate as stated earlier.
Randomization	Tumor-bearing mice were randomized at the time when treatment started based on tumor size, and age. For in vitro experiments, no randomization is needed since the cells treated are from the same batch.
Blinding	The tumor measurement was performed with cage labels blinded for treatments. The treatments were performed after the tumor measurement. For in vitro experiments, experiments execution and analysis was performed by different people in the lab.

The researchers involved in the bioinformatics analysis of the study (SN, LG, MM) were blinded to sample allocation and initial analyses/ sample processing wherever applicable.

Reporting for specific materials, systems and methods

We require information from authors about some types of materials, experimental systems and methods used in many studies. Here, indicate whether each material, system or method listed is relevant to your study. If you are not sure if a list item applies to your research, read the appropriate section before selecting a response.

Materials & experimental systems

n/a	Involved in the study
☐	☒ Antibodies
☐	☒ Eukaryotic cell lines
☒	☐ Palaeontology and archaeology
☐	☒ Animals and other organisms
☐	☒ Human research participants
☒	☐ Clinical data
☒	☐ Dual use research of concern

Methods

n/a	Involved in the study
☒	☐ ChIP-seq
☐	☒ Flow cytometry
☒	☐ MRI-based neuroimaging

Antibodies

Antibodies used

For flowcytometry, all antibodies were used at a 1:200 dilution unless otherwise mentioned.
eBioscience™ Fixable Viability Dye eFluor™ 780: Company: Invitrogen Catalog No. 65-0865-18 Lot No. 2365394 1:500
P1A-tetramer-PE: homemade 1:50
anti-CD45-antibody-Alexa Fluo700: Company: Biolegend Clone: 30-F11 Catalog No. 103128 Lot No. B327672
anti-CD45-antibody-PerCP: Company: Biolegend Clone: 30-F11 Catalog No. 103130 Lot No. B349380
anti-CD8-antibody-Brilliant Violet 421: Company: Biolegend Clone: 53-6.7 Catalog No: 100738 Lot No: B308976
Annexin V-APC: Company: Biolegend Catalog No: 640941 Lot No: B284206 1:100
Anti-CD11b-antibody-Brilliant Violet 711: Company: Biolegend Clone:M1/70 Catalog No: 101242 Lot No: B305910
Anti-CD11c-antibody-Brilliant Violet 421: Company: Biolegend Clone: N418 Catalog No: 117330 Lot No: B294539
F4/80-antibody-PE: Company: Biolegend Clone: BM8 Catalog No: 123110 Lot No: B281021
F4/80-antibody-Brilliant Violet 510: Company: Biolegend Clone: BM8 Catalog No: 123135 Lot No: B372803
MHC Class II-antibody-APC: Company: Biolegend Clone: M5/114.15.2 Catalog No: 107614 Lot No: B255462 1:500
Anti-CD69-antibody-FITC: Company:Biolegend Clone: H1.2F3 Catalog No: 104506 Lot No: B245589
Ly6G-antibody-Brilliant Violet 510: Company: Biolegend Clone: 1A8 Catalog No: 127633 Lot No: B307304
Ly6C antibody-PerCP: Company: Biolegend Clone: HK1.4 Catalog No: 128028 Lot No: B292026
Gr1-antibody-APC: Company: Biolegend Clone: RB6-8C5 Catalog No: 108412 Lot No: B297469
PD-L1-antibody-PE: Company: Biolegend Clone: 10F.9G2 Catalog No: 124308 Lot No: B340262
PD-1-antibody-FITC: Company: Biolegend Clone: 29F.1A12 Catalog No: 135214 Lot No: B347313
CD45.1-antibody-Brilliant Violet 510: Company: Biolegend Clone: A20 Catalog No: 110741 Lot No: B312868
TNFa-antibody-Brilliant Violet 711: Company: Biolegend Clone:MP6-XT22 Catalog No: 506349 Lot No: B343621
IFNg-antibody-APC: Company: Biolegend Clone:XMG1.2 Catalog No: 505810 Lot No: B335090
CD4-antibody-PerCP: Company: Biolegend Clone:RM4-5 Catalog No: 100538 Lot No: B283419
Lamp1-antibody-APC: Company: Biolegend Clone:1D4B Catalog No: 121614 Lot No: B292364

For western blot: all antibodies were used at 1:1000 dilution except for the secondary antibody which was used at 1:2500 dilution.
P-Creb-antibody: Company: Cell signaling Clone:87G3 Catalog No: 9198 Lot No: 18
Creb-antibody: Company: Cell signaling Clone:48H2 Catalog No: 9197 Lot No: 17
beta-actin-antibody: Company: Cell signaling Clone:13E5 Catalog No: 5125 Lot No: 6
Anti-rabbit IgG, HRP-linked Antibody: Company Cell signaling Catalog No:7074 Lot No:31

The following antibodies were used for in vivo treatment
anti-CTLA4 blocking antibody: Company: BioXcell Clone 9H10 Catalog #BE0131 (40 µg per mouse)
anti-PD-1 blocking antibody: Company: BioXcell Clone RMP1-14 Catalog #BE0146 Lot No: 695318A1 (200 µg per mouse)
anti-CD4 depletion antibody: Company: Biolegend Clone GK1.5 Catalog #100402 (500 µg per mouse)
anti-CD8 depletion antibody: Compnay: BioXCell, Clone mAb 53-6.7 Catalog #BE0004-1 Lot No: 705020N1 (500 µg per mouse)
anti-MHC II blocking antibody: Company: BioXcell, Clone Y-3P Catalog #BE0178 Lot No:796422M2 (500 µg per mouse)
InVivoMAb rat IgG2b isotype control: Company: BioXcell Catalog #BE0090
InVivoMAb rat IgG2a isotype control: Company: BioXcell Catalog #BE0089
InVivoMAb polyclonal Syrian hamster IgG: Company: BioXcell Catalog #BE0087

Validation

All antibodies are validated by the manufacturer except for P1A-tetramer which was used to stain TCRP1A CD8 T cells for validation of specificity.

eBioscience Fixable Viability Dye eFluor 780 Validation: BALB/c thymocytes were uncultured (left) or cultured overnight at 37 degree and then stained with Fixable Viability Dye eFluor780.

P1A-tetramer Validation: The antibody was used to stain TCRP1A CD8 T cells for validation of specificity.
anti-CD45 antibody Validation: C57BL/6 mouse splenocytes stained for validation.
anti-CD8 antibody Validation: C57BL/6 mouse splenocytes were stained for validation
Annexin V-APC Validation: T cells were irradiated and stained with Annexin V-APC
Anti-CD11b antibody Validation: C57BL/6 mouse bone marrow cells were stained with CD11b Brilliant Violet 711.
Anti-CD11c antibody Validation: C57BL/6 mouse splenocytes were stained with mouse I-A/I-E FITC and CD11c (clone N418) Brilliant Violet 421 or Armenian hamster IgG Brilliant Violet 421 isotype control for validation.
F4/80 antibody Validation: Thioglycolate-elicited BALB/c mouse peritoneal macrophages was stained with BM8 PE for validation.
MHC Class II antibody Validation: C57BL/6 mouse splenocytes were stained with anti-mouse I-A/I-E (clone M5/114.15.2)APC or rat IgG2b, APC isotype control for Validation.
Anti-CD69 antibody Validation: PMA-stimulated splenocytes were stained with H1.2F3 FITC for validation.
Ly6G antibody Validation: C57BL/6 mouse bone marrow cells were stained with Ly-6G (clone 1A8) Brilliant Violet 510 or rat IgG2a, Brilliant Violet 510 isotype control for validation.
Ly6C antibody Validation: C57BL/6 bone marrow cells were stained with Ly-6C (clone HK1.4) PerCP for validation.
Gr1-antibody Validation: C57BL/6 mouse bone marrow cells were stained with Ly-6G/Ly-6C APC (clone RB6-8C5) or APC Rat IgG2b, isotype control for validation.
PD-L1-antibody Validation: C57/B6 mouse splenocytes were stained with anti-CD274 (clone 10F.9G2) PE or rat IgG2b
PD-1-antibody Validation: Con-A and IL-2 stimulated C57BL/6 mouse splenocytes were stained with CD3 APC and CD279 (clone 29F.1Al2) FITC or rat IgG2a, FITC isotype control.
CD45.1-antibody Validation: Splenocytes from Ly5.1 mice splenocytes were stained with CD45.1 (clone A20) Brilliant Violet 510'm or mouse IgG2a Brilliant Violet 510 isotype control.
TNFa-antibody Validation: PMA+ Ionomycin-stimulated (six hours) C57BL/6 mouse splenocytes were surface stained with CD3 APC and then intracellularly stained with TNF- (clone MP6-XT22) Brilliant Violet 711 or rat IgG1, Brilliant Violet 711.
IFNg-antibody Validation: PMA/Ionomycin-stimulated C57BL/6 mouse splenocytes stained with XMG1.2 APC and B220 (RA3-6B2) PE
CD4-antibody Validation:C57BL/6 mouse splenocytes stained with CD4 (clone RM4-5) PerCP or rat IgG2a, PerCP isotype control.
Lamp1-antibody Validation: Balb/c peritoneal macrophages stained with 1D4B APC
P-Creb-antibody Validation: Western blot analysis of extracts from SK-N-MC cells, untreated or forskolin- and FGF-treated, using Phospho-CREB (Ser133) (8763) Rabbit mAb or CREB (48H2) Rabbit mAb #9197.
Creb-antibody Validation: Western Blot analysis of extracts from SK-N-MC, COS, NIH/3T3, C6 and Drosophila S2 cells, using CREB (48H2) Rabbit mAb.
b-actin Validation: Western blot analysis of extracts from various cell lines using -Actin (13E5) Rabbit mAb (HRP Conjugate).
anti-CTLA4 blocking antibody validation: the use of the antibody is cited by multiple articles listed at: https://bioxcell.com/invivomab-anti-mouse-ctla-4-cd152-be0131
anti-PD-1 blocking antibody validation: the use of the antibody is cited by multiple articles listed at:https://bioxcell.com/invivomab-anti-mouse-pd-1-cd279-be0146
anti-CD4 depletion antibody validation: the use of the antibody is cited by multiple articles listed at:https://bioxcell.com/invivomab-anti-mouse-cd4-be0003-1
anti-CD8 depletion antibody validation: the use of the antibody is cited by multiple articles listed at:https://bioxcell.com/invivomab-anti-mouse-cd8a-be0004-1
anti-MHC II blocking antibody validation: the use of the antibody is cited by multiple articles listed at:https://bioxcell.com/invivomab-anti-mouse-cd8a-be0004-1
InVivoMAb rat IgG2b isotype control validation: the use of the antibody is cited by multiple articles listed at: https://bioxcell.com/invivomab-rat-igg2b-isotype-control-anti-keyhole-limpet-hemocyanin-be0090#tab_references
InVivoMAb rat IgG2a isotype control validation: the use of the antibody is cited by multiple articles listed at: https://bioxcell.com/invivomab-rat-igg2a-isotype-control-anti-trinitrophenol-be0089
InVivoMAb polyclonal Syrian hamster IgG validation: the use of the antibody is cited by multiple articles listed at:https://bioxcell.com/invivomab-polyclonal-syrian-hamster-igg-be0087

Eukaryotic cell lines

Policy information about cell lines

Cell line source(s)

CT26: ACTT CRL-2638
B16-F1: ATCC, CRL-6323
B16F10-OVA: ATCC, CRL-6475, the OVA protein was introduced in the lab.
HEPA1-6: ATCC CRL-1830
J558: ATCC TIB-6
TC-1: was kindly provided by C. Gérard (GlaxoSmithKline Biologicals, Rixensart, Belgium).
4T1: ATCC, CRL-2539
Renca: ATCC CRL-2947
E.G7-OVA: a kind gift from Prof. J. Vanginderachter, VUB, Belgium
LS411N: a kind gift from Prof. N. Odartchenko, CHUV, department of Surgery, Lausanne, Switzerland.
TS/A cells: a kind gift from Prof. G. Prodi, University of Bologna, Bologna, Italy
CMS5a cell line: was obtained from the lab of H. Shiku (Mie University School of Medicine, Japan).
SK-OV-3: CLS, Cryovial: 300342
PC-3 ATCC CRL-1435
T429.6: a cell line derived from induced TiRP melanoma tumor model in the lab. (PMID: 29123081)
MC38 and MC38-OVA: the MC38 cell line was kindly provided by M. Waldner, University of Erlangen, Germany. The plasmid encoding chicken ovalbumin protein was transduced into the MC38 cell line in the lab.

Authentication	The cell authentication for all murine cell lines was performed by ATCC cell line authentication service using short tandem repeat (STR) profiling in 2022. All human cell lines were validated by Eurofin Cell lline Authentication Service using PCR-single-locus-technology in 2023.
Mycoplasma contamination	All cell lines used were regularly tested (every one month and half) and are negative for mycoplasma
Commonly misidentified lines (See ICLAC register)	No

Animals and other organisms

Policy information about studies involving animals; ARRIVE guidelines recommended for reporting animal research

Laboratory animals	All mice were housed at an ambient temperature around 21-23 C°, humidity of 40-60% and a light dark cycle of 12 hours. TiRP mice: TiRP mice have been created by crossing Ink4a/Arfflox/flox mice with mice carrying a transgenic construct controlled by the tyrosinase promoter and driving the expression of H-Ras12V and Trap1a which encodes a MAGE-type tumor antigen P1A. Females mice with age between 10-18 weeks were used. TCR-P1A mice: TCRP1A mice heterozygous for the H 2Ld/P1A35-43-specific TCR transgene were kept on the B10.D2;Rag1−/− background, only female mice between age 9-12 were used; TCR-OT-I mice:Only female mice between age 9-12 were used; TCR-OT-II mice:Only female mice between age 9-12 were used; NSG mice: Females mice with age between 8-14 weeks were used. C57BL/6J mice: Female mice with age between 6-12 weeks were used. BALB/c mice: Female mice with age between 6-12 weeks were used. Adra2a-KO mice: Female mice with age between 6-12 weeks were used. Adrb1/b2-KO mice: Female mice with age between 6-12 weeks were used. DBA/2 mice: Both female and male mice with age between 6-12 weeks were used. Ly5.1 mice: Female mice with age between 6-12 weeks were used.
Wild animals	No
Field-collected samples	No
Ethics oversight	All mice used in this study were produced under specific pathogen free (SPF) conditions at the animal facility of the de Duve Institute. All the rules concerning animal welfare have been respected according to the 2010/63/EU Directive. All procedures were performed with the approval of the local Animal Ethical Committee (UCLouvain university, Belgium), with reference 2015/UCL/MD/14 and 2019/UCL/MD/24.

Note that full information on the approval of the study protocol must also be provided in the manuscript.

Human research participants

Policy information about studies involving human research participants

Population characteristics	Human PBMCs isolated from haemochromatosis patients were used for reconstitution of the murine xenograft.
Recruitment	Only PBMC samples from patients with allogeneic HLAs to the tumour cell lines used in this study were used.
Ethics oversight	The study protocol was approved by "UCLouvain commission d'éthique hospitalo-facultaire" under authorisation approval n° CEHF 2021/13SEP/373. The ethical approval encompasses an exemption of informed consent based on the fact that we only use blood that qualifies as “Residual Human Body Material”, which needs to be collected as a therapeutic measure for hemochromatosis patients. The absence of “opting out” option was checked for all patients.

Note that full information on the approval of the study protocol must also be provided in the manuscript.

Flow Cytometry

Plots

Confirm that:

☒ The axis labels state the marker and fluorochrome used (e.g. CD4-FITC).

☒ The axis scales are clearly visible. Include numbers along axes only for bottom left plot of group (a 'group' is an analysis of identical markers).

☒ All plots are contour plots with outliers or pseudocolor plots.

☒ A numerical value for number of cells or percentage (with statistics) is provided.

Methodology

Sample preparation	Tumors and spleens were isolated from tumor-bearing mice. The tumor samples were dissociated by using a cocktail of three enzymes (Collagenase I, Collagenase II and Dispase) with the help of gentle macs dissociator. Spleens were gently smashed in cell culture medium to generate cell suspension. Single cells were obtained by filtration of tissue homogenate through a 40-

	uM filter. Spleen samples were simply grinded gently with the flat end of a syringe in full T cell culture medium. The cell suspensions were collected and filtered through a 70 micrometer filter (#352350, FALCON).
Instrument	BD LSRFortessa
Software	Flowjo 10.7.2
Cell population abundance	Facs sorting was performed to isolate macrophages, T cells and MDSCs for QPCR analysis. Post Facs sorting, we obtained the following number of cells: macrophages (around 500,000 cells, purity 96%), MDSCs (around 450,000 cells, purity 95%) and CD8+ T cells (around 250,000 cells, purity 92%).
Gating strategy	Gating strategy on Spleen and tumor tissues: 1. FSC and SSC 2. FSC-H and FSC-A to gate on single cell population 3. Viability 780 to gate on live cells, this is defined as Viability 780 negative cells. 4. CD45+ cells 8. CD8+ cells for T cells, Annexin V staining was gated on CD8+ cells population, the threshold was placed based on negative controls. 9. CD11b+ Gr1+ cells for Myeloid cells, which was further gated on Ly6C high Ly6G low or Ly6C low Ly6G high population for MMDSC and PMN MDSC respectively. Annexin V staining on these cells were gated based on control cells. 10. F4/80+ CD11b+ for macrophages. The expression of MHC II was analysed by medium fluorescence intensity. The gating strategy is shown on Extended Data Figure 2 d-h.

☒ Tick this box to confirm that a figure exemplifying the gating strategy is provided in the Supplementary Information.